Deflection of Ag- atoms in an Inhomogeneous Magnetic Field

by
Bonginkosi Vincent Kheswa

Thesis presented in partial fulfilment of the requirements for the degree Master of Science at the University of Stellenbosch

Supervisor: Dr Paul Papka
Co-supervisor: Mr Robert Thomas Dobson
Faculty of Science
Department of Physics

December 2011

Declaration

By submitting this thesis/dissertation electronically, I declare that the entirety of the work contained therein is my own, original work, that I am the sole author thereof (save to the extent explicitly otherwise stated), that reproduction and publication thereof by Stellenbosch University will not infringe any third party rights and that I have not previously in its entirety or in part submitted it for obtaining any qualification.

December 2011

Abstract

In the current design of the high temperature gas cooled reactor, a small fraction of coated fuel particles will be defective. Hence, ^{110}Ag may be released from the fuel spheres into the coolant gas (helium) and plate out on the cooler surfaces of the main power system. This poses a radiation risk to operating personnel as well as general public.

The objectives of this thesis were to design and construct an apparatus in which silver-109 atoms may be produced and deflected in an inhomogeneous and homogeneous magnetic field, compare experimental and theoretical results, and make a recommendation based on the findings of this thesis to the idea of removing silver-110 atoms from the helium fluid by deflecting them with an inhomogeneous magnetic field onto target plates situated on the inner perimeter of a helium pipe.

The experimental results for the deflection of the collimated Ag- atoms with the round-hole collimators showed a deflection of 1.77^{o} and 2.05^{o} of the Ag- atoms due to an inhomogeneous magnetic field when the target plate was positioned 13 and 30 mm away from the magnet, respectively. These values were considerably greater than the theoretical deflection of 0.01^{o} and 0.02^{o} that were calculated for the average velocity of atoms, $\bar{v}$ = 500 m/s. The case where Ag- atoms were collimated with a pair of slits and the target plate positioned 13 mm away from the magnet showed the following: An inhomogeneous magnetic field changes the rectangular shape of the beam to a roughly elliptical shape. The beam of Ag- atoms was not split into two separate beams. This was caused by the beam of Ag- atoms consisting of atoms travelling at different speeds. The maximum deflection of Ag- atoms was 1.16^{o} in the *z* direction and 1.12^{o} in the *x* direction. These values were also significantly greater than 0.01 mm calculated at $\bar{v}$ = 500 m/s. This huge difference between the theoretical and experimental results raised a conclusion that the size of each Ag deposit depended mostly on the exposure time that was given to it. It was noticed that the beam of Ag- atoms was not split into two separate beams, in both cases.

The conclusion was that the technique of removing Ag- atoms from the helium stream by means of an inhomogeneous magnetic field may not be effective. This is due to the inability of the inhomogeneous magnetic field to split the beam of Ag- atoms into two separate beams in a vacuum of ~10^{-5} mbar. It would be even more difficult for an inhomogeneous magnetic field to split the beam of Ag- atoms in helium, due to the Ag- atoms having a shorter mean free path in helium compared to a vacuum.

Opsomming

In die huidige ontwerp van die hoë temperatuur gas afgekoelde reaktor, is 'n klein fraksie van omhulde brandstof deeltjies foutief. ^{110}Ag kan dus vrygestel word vanaf die brandstof sfere in die verkoelingsgas (helium) wat dan op die koeler oppervlaktes van die hoofkragstelsel presipiteer. Hierdie ^{110}Ag deeltjies hou 'n bestraling risiko vir die bedryfpersoneel sowel as vir die algemene publiek in.

Die doelwitte van hierdie verhandeling is eerstens om 'n apparaat te ontwerp en konstrueer wat silwer-109 atome produseer en nie-homogene en homogene magnetiese velde deflekteer,. Tweedens om die eksperimentele en teoretiese resultate met mekaar te vergelyk. Derdens om 'n aanbeveling te maak gebasseer op die bevindinge van hierdie verhandeling rakende die verwydering van silwer-110 atome uit die helium vloeistof deur hulle met 'n nie-homogene magneetveld te deflekteer op die teikenplate binne-in ' n helium pyp.

Die eksperimentele resultate vir die defleksie van die gekollimeerde Ag-atome met die ronde gat kollimators toon ‘n defleksie van 1.77^{o} en 2.05^{o} van die Ag-atome as gevolg van ‘n nie-homogene magneetveld wanneer die teikenplaat 13 mm en 30 mm, onderskeidelik, vanaf die magneet geposisioneer is. Hierdie waardes is aansienlik groter as die teoretiese defleksies van 0.01^{o} en 0.02^{o} wat bereken is vir ‘n gemiddelde snelheid van 500 m/s vir die atome. Die geval waar Ag-atome met 'n paar splete gekollimeer is en die teikenplaat 13 mm weg van magneet geposisioneer is, is die volgende resultate verkry: 'n nie-homogene magneetveld verander die reghoekige vorm van die bondel na 'n rowwe elliptiese vorm. Die bondel Ag-atome is nie volkome twee afsonderlike bundels verdeel nie. Dit is omdat die bondel van Ag-atome bestaan uit atome wat teen verskillende snelhede beweeg. Die maksimum defleksie van Ag-atome is 1.16^{o} in die z-rigting en 1.12^{o} in die x-rigting. Hierdie waardes is ook aansienlik groter as 0.01^{o} bereken teen 500 m/s. Hierdie groot verskil tussen die teoretiese en eksperimentele resultate dui daarop dat die grootte van elke Ag neerslag grootliks afhanklik is van die blootstellingstyd wat daaraan gegee is. Daar is vasgestel dat die straal van Ag-atome in beide gevalle nie in twee afsonderlike bondels verdeel nie.

Die gevolgtrekking is dat die tegniek van die verwydering van Ag-atome uit die helium stroom deur middel van 'n nie-homogene magneetveld nie effektief is nie. Dit is te wyte aan die onvermoë van die nie-homogene magneetveld om die bondel Ag-atome te verdeel in twee afsonderlike bondels in 'n vakuum van ~ 10^{-5} mbar. Dit sou selfs nog moeiliker vir 'n nie-homogene magnetiese veld wees om die bundel Ag-atome in helium te verdeel, weens die korter gemiddelde beskikbare pad van Ag-atome in helium wanneer dit met 'n vakuum vergelyk word.

Dedicated to my parents, Johnson and Tholiwe Kheswa

Acknowledgements

I am grateful to the following people:

All the members of the MaNus-MatSci (Masters in Accelerator and Nuclear/Material Sciences) Programme at the universities of Zululand, Western Cape and Stellenbosch for providing me with such a memorable study opportunity

PBMR (Pty) Ltd for the munificent financial support for this project, and iThemba Labs and NRF for their special financial support during the first year of my master's studies, which prepared me for this momentous project

My supervisors, Mr R T Dobson and Dr P Papka, for their comments on the manuscript and for their suggestions for further reading

The Department of Mechanical Engineering, especially Ockert Kritzinger, for the design drawings, suggestion on a set-up of the experiments and technical assistance

The Department of Electrical Engineering, at Stellenbosch University, especially Dr Roger Wang, for advising me to use MagNet software in order to find a best geometry of the magnetic circuit to produce an inhomogeneous magnetic field in the gap

Dr Rainer W Thomae, senior accelerator physicist from iThemba LABS, for his time, kindness, expertise and great contribution to the accomplishment of this work

Contents

Page

List of figures

Page

List of tables

Page

Nomenclature

Abbreviations

HTGR	High temperature gas-cooled reactor
MPS	Main power system
PBMR	Pebble bed modular reactor
Triso	Tristructural- isotropic

Roman letters

A	Area, m^2
B	Magnetic flux density, T
C	Cross-sectional perimeter, m
F	Deflecting force, N, total angular momentum of an atom
f	Quantum number of the total angular momentum of an atom
H	Magnetic field intensity, A.m
$\hbar$	Unit of an angular momentum, Js
I	Nuclear angular momentum
i	Nuclear angular momentum quantum number
J	Total angular momentum of an electron
j	Total angular momentum quantum number of an electron
K	Dimensionless leakage factor
L	Orbital angular momentum of an electron
l	Length, m, orbital angular momentum quantum number of an electron
m	Mass, kg, magnetic quantum number
r	Radius, m
S	Spin angular momentum
T	Temperature, °C
t	Time, s
U	Potential energy, eV
V	Reluctance drop, $s^2.A^2/kg.m$
v	Velocity, m/s
z	Distance, m

Greek letters

μ	Magnetic dipole moment, $A.m^2$
τ	Angular velocity, Nm
ω	Torque, radians per second

Subscripts

B	Magnetic field
d	Magnet
e	Electron
f	Total angular momentum of an atom
g	Gap

m	Magnet
mg	Between the target and magnet
mp	Most probable
n	Nuclear
p	Proton
s	Spin angular momentum
z	z direction in the xyz plane

Constants

Boltzmann constant, $k = 1.38066 \times 10^{-23}$ J/K
Bohr magneton, $\mu_B = 9.270154 \times 10^{-24}$ J/T
Plank's constant, $\hbar = 1.054571628 \times 10^{-34}$ Js

1 CHAPTER 1

INTRODUCTION

The key design characteristic of high temperature gas-cooled reactors (HTGRs) such as the pebble bed modular reactor (PBMR) is the use of tristructural- isotropic (Triso)-coated fuel particles and helium coolant [Po03]. The preferred coolant, helium, does not absorb neutrons or impurities. It is therefore, better than water, because it does not become radioactive. It also remains in gaseous phase under all conditions in the reactor. These concepts provide the potential for increased energy conversion efficiency and for high-temperature process heat applications, such as coal gasification or thermochemical hydrogen production. While all the gas-cooled reactor concepts have sufficiently high temperature to support process heat applications, such as desalination processes, as well as some thermochemical processes of interest to alternative fuel production, the higher temperatures of HTGRs open a broader and more efficient range of applications.

HTGRs require substantive improvements in fuel design, especially as regards material properties [Me08]. The benefit of these developments is not restricted to dedicated HTGR applications, but is valid for all kinds of high temperature reactor applications irrespective of the core design. As a result, the HTGR concepts and applications can be taken primarily as an important direction for innovative, long-term future research and development. Licensing requirements for modern nuclear reactors are becoming increasingly stringent; therefore analysis of reactors must become more and more detailed and accurate.

HTGRs, if correctly designed, have the intrinsic ability to preserve structural integrity of the reactor internals and fuel elements during all realistically anticipated accident conditions**.** However, fission products are not completely retained in the fuel elements during normal operation, and during accident conditions, release from fuel elements may be accelerated. Although the release of fission products from the fuel is only a small fraction of the total inventory, it still presents a radiological risk to operating personnel during operation and to the general public after accidents. When fission products are deposited, whether directly plated out on cooler metallic surfaces, or carried by dust in the coolant gas stream, radiation fields result, which limit personnel access and exposure times to perform required maintenance work.

Major accidents usually entail a pipe break in the main power system, followed by the rapid or slow depressurisation (depending on the size of the pipe break) of coolant gas from the main power system and reactor cavity [Me04]. This depressurisation lifts fission products attached to dust and plated out in cooler regions, and transports them to the environment. Dust production and plate out/lift- off are very difficult to mitigate; therefore one of the practical methods to decrease the radiation fields in the plant and possible releases to the environment is to limit the loss from fuel elements. Fission products that are, formed during the operation of an HTGR, and are not retained in the uranium oxide kernel may be released from the fuel spheres as a result

of failure of the Triso-particle layers during extreme events [Li06]. Long- lived fission products may also diffuse through intact Triso-particle layers (albeit very slowly) or may form outside the Triso-particle due to uranium and thorium contamination of the fuel sphere matrix material.

Fission products are transported from the fission sites, through the fuel materials to the surface of the fuel spheres, where they are desorbed into the coolant gas. These released fission products either plate out on the cooler surfaces of the main power system (metal and halogen fission products) or remain in the coolant gas. This poses a risk to operating personnel who may need to access components for maintenance purposes, which increases the decontamination requirements for the plant. During accidents, where coolant gas escapes from the primary circuit into the containment building, fission products can be transported to operating personnel and to the general public. It is therefore vital to study how fission products can be removed from the reactor before they reach either workers or the general public.

In this study, a specially designed apparatus was built to check the efficiency of an inhomogeneous magnetic field generated by permanent magnets in removing Ag- atoms (one of the metallic fission products) from the reactor coolant. In an actual HTGR, the permanent magnets would be placed in the hot outlet pipe, termed the hot-pipe, as illustrated in Figure 1.1. Within the hot-pipe there would be a multi-layer deposition ring forming an inner lining to the hot-pipe. The Ag- atoms within the hot-pipe would be deflected by an inhomogeneous magnetic field and would be deposited onto the multi-layer deposition ring. The multilayer deposition ring is made up of three layers: the outer layer, (made of a material, such as SiC, that is diffusion- resistant to the fission products); the binding layer of a fission product, (such as Cr alloy); and an inner layer acting as a landing zone for fission products, (such as graphite). This structure can be removed at the end of the HTGR lifecycle and sent for long-term storage.

To check the efficiency of an inhomogeneous magnetic field in this study, a specially designed magnetic circuit was used to produce a magnetic field in the gap. A beam of Ag- atoms generated in a crucible was collimated with a pair of collimators to the gap of the magnetic circuit perpendicular to the magnetic field lines. As a result, the beam was deflected to a specified target plate. For safety purposes, ^{109}Ag was used instead of ^{110}Ag, which is radioactive. The experiments were run in vacuum to investigate the efficiency of an inhomogeneous magnetic field in vacuum first, before it is investigated in helium. ^{137}Cs is another radioactive metallic fission product released from the fuel spheres. According to the Stern-Gerlach principle, an atom should have one valance electron in order to be deflected in an inhomogeneous magnetic field. It follows that it is in principle possible to deflect ^{137}Cs.

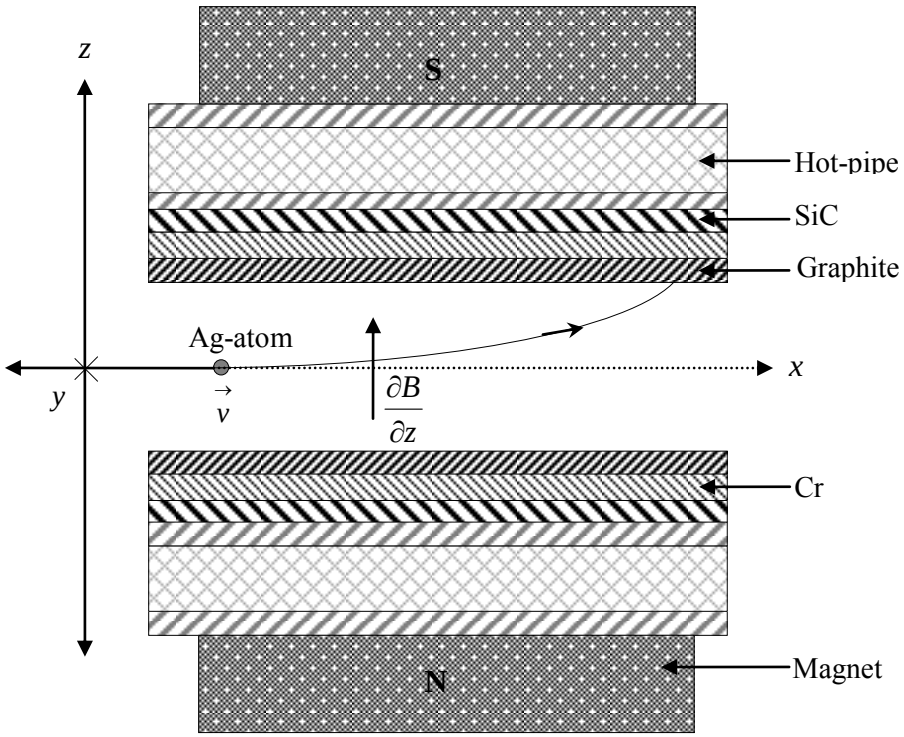

Figure 1.1: Cross- section of the hot-pipe

To summarise: This project is part of a much larger project in which removal of unwanted particles from the hot coolant as it leaves the reactor pressure vessel is being investigated. Of these unwanted particles, radioactive ^{110}Ag is particularly worrisome; its half-life is long (249.79 days) and this had delayed-maintenance and personal safety implications. Further, this project has the following specific objectives:

i. To design and construct the apparatus in which
ii. silver-109 atoms may be produced and deflected in a magnetic field using permanent magnets and a magnetic circuit capable of producing a homogeneous and an inhomogeneous magnetic field.
iii. To collect the atoms after being deflected onto a target
iv. To record the experimental deflection results and compare them with theoretically predicted results
v. To make recommendation based on the findings of this project in relation to the larger project (of removing unwanted particles from the hot coolant as it leaves the reactor pressure vessel)

2 CHAPTER 2

LITERATURE STUDY

The background of this study is provided in this chapter. The main focus is on nuclear fission, nuclear radiations and their biological effects, PBMR fuel particles, release of silver in a PBMR and the Stern-Gerlach principle.

2.1 Nuclear fission

A naturally occurring isotope, ^{235}U can absorb a neutron to form an unstable nuclide, ^{236}U, with large cross- section for neutrons with the energy of E_n ~ 25 MeV. The compound nucleus, ^{236}U, decays via γ- ray emission with a ratio of 14%. In its ground state, this nucleus decays via α emission with a half- life of 2.4 x10^7 years. In the remaining 86% of the cases, the absorption of a slow neutron by ^{235}U results in the production of the unstable ^{236}U nuclide. This ^{236}U has opposing forces of two positively charged nuclides. As a result, it splits into two fragments (not necessarily of equal mass), with the liberation of energy approximately equal to the product of the mass number (236) and the binding energy per nucleon (0.9 MeV), which is approximately 200 MeV [Sh02]. The general fission reaction of ^{235}U may be illustrated by

$$^{235}U + n \rightarrow X + Y + Nn + E \qquad 2.1$$

Equation 2.1 represents the fission of one atom of ^{235}U induced by one thermal neutron n to yield the release of fission products X and Y of varying masses plus an average of $N = 2.42$ neutrons and overall release energy of E_n ~ 200 MeV. From this energy, 166 MeV is released in the form of kinetic energy of the two fission fragments [Mu01]. The remaining energy is shared among the emitted neutrons, with prompt γ radiation accompanying fission and the rest of the energy emanating from the decay of the fission products through β emission, followed by γ radiation and emission of decayed neutrons.

When a sample of ^{235}U is bombarded with slow neutrons, the fission products are rarely of equal mass. The intermediate nuclide ^{236}U breaks into fragments in as many as approximately 30 different pairs, producing 60 different fission fragments. The most common fission fragments have a mass ratio of 3:2 [La03]. Neutrons emitted from the fission process are classified as fast neutrons varying in energy over the range, with 2 MeV as the average energy. Due to the release of more than one neutron per fission, a self-sustaining chain reaction is possible that liberates considerable energy, forming the basis of the nuclear reactor as a principal source of neutrons and energy. In the case of ^{235}U, slow neutrons are required for neutron absorption and fission to occur. As a result, a nuclear reactor is equipped with a moderator such as graphite or water that can reduce the energies of fast neutrons via elastic scattering of the neutrons with atoms of low atomic weight.

Two other isotopes of uranium are also found to be fissionable, namely ^{238}U and ^{233}U [Sl55]. The common isotope ^{238}U captures the neutron and becomes ^{239}U, which decays by β emission to ^{239}Np. ^{239}Np has a half-life of only 2.3 days and decays by another β emission to ^{239}Pu [Su84]. These isotopes are produced through nuclear reaction.

Plutonium-239 is a long- lived radioactive nuclide with a half- life of approximately $2.4x10^4$ years [Sl55]. It decays to ^{235}U by emitting an α- particle (^4He). However, ^{239}Pu is also found to be fissionable by slow neutrons, just as ^{235}U is. Thus arises the possibility of converting the common, non-fissionable isotope of ^{238}U into fissionable isotope ^{239}Pu. This possibility has been the basis of much of the work on nuclear energy, as there is not enough ^{235}U in nature to provide a very extensive source of energy. Another similar reaction starts with thorium, which is also fairly common in nature. When ^{232}Th is bombarded with slow neutrons, it absorbs a neutron and becomes ^{233}Th, which is fissionable by slow neutrons. On account of the fair abundance of thorium, this is a useful reaction.

In addition to these nuclei that are fissionable by slow neutrons, there are number of heavy isotopes that are fissionable by fast neutrons which energies of millions of electron volts [Sl95]**.**

2.2 Nuclear radiations

Radiation is a form of energy that is used in a wide number of applications for a variety of purposes, such as radiotherapy and diagnosis (the main medical applications) [Lo79]. Radiation is used in radiotherapy for the treatment of malignant diseases, without producing harmful effects in healthy tissues. Radiation is used in diagnosis for investigating the patient's conditions through the distribution of a suitable radioactive material introduced into the body. However, as with the other forms of energy, it can be harmful when uncontrolled [Sa68]. To control radiation it is necessary to understand its nature. In the broad sense, nuclear radiations include γ- rays, β- particles, α- particles and many other forms. However, the immediate interest of this study is limited to γ- rays and β -particles, which are the types of radiation that are emitted from the decay of ^{110}Ag.

2.2.1 Gamma radiation

The γ-rays are high-energy photons that originate from transitions between the energy levels within the atomic nucleus [Ho78]. For instance, ^{110}Ag decays via β emission to unstable ^{110}Cd, and the excess energy of the ^{110}Cd is released in the form of γ radiation [Mo02]. Because γ radiation has neither charge nor mass, this brings about no change in the atomic number or atomic weight of the emitting isotope [Sa68]. The energies of the γ- rays are mostly in the range of few keV to few MeV. They are very penetrating. Absorbing materials, such as the human body, cannot completely stop γ- rays, but can reduce their intensity.

2.2.2 Beta radiation

Atoms emit β radiation through a process known as β decay. A β decay occurs when an atom has either too many protons (positively charged particles) or too many neutrons (electrically neutral particles) in its nucleus. When this occurs, a force, called the weak nuclear force, causes the unstable atom to change an extra proton into a neutron, or vice versa, and become more stable [Hi92]. This β decay can produce positive or negative particles. In positive β decay, a proton in an unstable nucleus turns into a neutron by emitting a positively charged β particle (positron) and an electron neutrino. Neutrinos have energies that range from nearly zero to large quantities. In negative β decay, a neutron in an unstable nucleus turns into a proton by emitting a negatively charged β particle (electron) and an antineutrino, the antimatter counterpart of the electron neutrino. Different radionuclides emit β radiation of different energies. The maximum energy given off in β decay of various radionuclides ranges between 0.018 MeV (for tritium) and 2.24 MeV (for ^{90}Sr) [Sh92].

2.2.3 Biological effects of β and γ radiations

The effects of radiation are largely based on the ionization produced when the energy is absorbed in matter [Sa68]. While some of the biological and even physical effects are understood, many of the biological mechanisms and the ultimate radiation damage in biological tissues are not understood. The γ- rays, because of their penetrating nature, may dissipate only a fraction of their energy in passing through the body [Sa68]. This is particularly true for high- energy rays. The energy dissipated is the dose delivered to the body or portion of the body. Radioisotopes, in contrast, may present a further hazard when the material is taken into the body and irradiates the tissues or organs internally. The β emitters can be both an internal and an external hazard. The range of most external β radiation is great enough that the outer tissues, at least, will be penetrated. The most common external effects are radiation burns and malignancies of the skin.

Moreover, there are many secondary effects that can be caused by ionization processes [Sa68]. They may disrupt molecules, they may destroy body cells or the energy may merely appear in the final form of heat released within the absorber. Depending on the location of the absorbing atom within the molecule, the ionization may or may not disrupt the molecule. The ability of the molecule to reproduce itself may be destroyed if the disrupted molecule is within the body cell. Many of these processes may be reversible; that is, damage caused to molecule or cell disruption can be reversed by the usual reparative mechanism of the body. However, in the case of a large acute dose or continued chronic exposure, there is the possibility that nonreversible damage will occur. Another type of cell change identified is the destruction of the regulative functions of tissues. In this case a carcinoma (cancer) may be produced.

2.3 The PBMR fuel particles

The most unique feature of the PBMR is its charge of 370, 000 fuel spheres (or pebbles), each containing Triso- coated particles, shown in Figure 2.1, where nuclear fission occurs [Sc05]. Each 60 mm diameter sphere is coated with a 5 mm thick graphite layer that is fuel- free. The graphite can withstand temperatures of 2 800 °C, which is much higher than the maximum 1 600 °C that the reaction can produce. Beneath this graphite layer, approximately 15,000 coated particles are embedded in a graphite matrix. Each particle is 0.92 mm in diameter, made of four layers of coatings and the 0.5 mm diameter uranium dioxide fuel kernel. The function of these coating layers is to retain fission products within the particle [Li06]. The porous carbon buffer maintains the shape of the fuel kernel as it undergoes deformation caused by density change due to the change of fuel material into fission products. It accommodates the fuel products without over- pressurising Triso- coated particles. The silicon carbon buffer coating layer gives mechanical strength to the Triso- coated particles and acts as a barrier to the fission products, which would diffuse easily through the inner pyrolytic coating layer. The 0.5 mm diameter uranium dioxide fuel kernel contains 8% to 10% enriched uranium ^{235}U [We01]. Natural uranium contains only 0.7% ^{235}U, which is the predominant fissionable isotope of natural uranium.

During PBMR operation, new and re- used fuel spheres are replenished at the top of the reactor as used fuel spheres are removed from the bottom of the reactor. As they leave the reactor, the used fuel spheres are measured for the amount of remaining fissionable material. If they are spent, they are automatically removed from the rotation and stored in a spent fuel storage facility. A fuel sphere will cycle the reactor approximately 10 times before going to the storage facility. The PBMR reactor uses approximately 10 to 15 complete loads of spheres in its lifetime. A fuel sphere will last approximately three years, while its in- active graphite moderator counterpart will last approximately twelve years [Sc05].

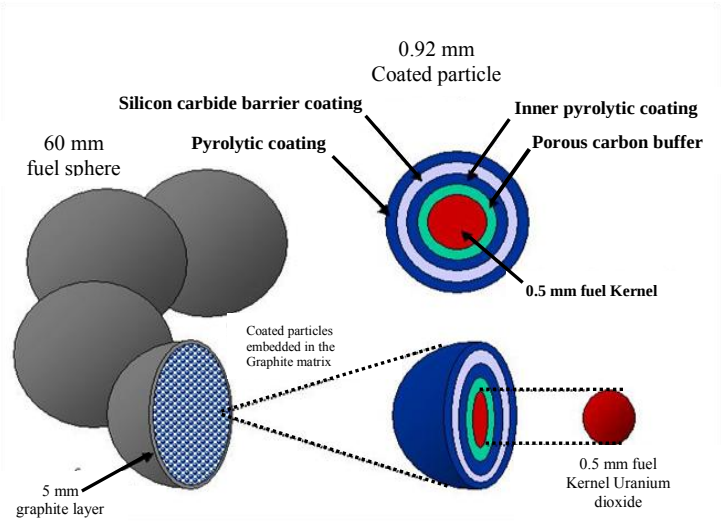

Figure 2.1: Pebble bed Triso fuel sphere cross- section [Sc05]

2.4 ^{110}Ag in PBMR

In the current PBMR design, the fuel spheres can be manufactured economically in large volumes, while maintaining fuel quality and integrity during manufacture and subsequent irradiation [Me04]. Even under the best manufacturing conditions, a small fraction of coated fuel particles will be defective. As a result, ^{110}Ag may be released from the fuel spheres into the coolant gas and plate out on the cooler surfaces of the main power system. Furthermore, under abnormally high temperatures and power surges, coated fuel particles may start to fail and increase the release of ^{110}Ag. As ^{110}Ag is one of the long- lived radioactive fission products, it poses a radiation risk to operating personnel who may need to access components for maintenance purposes and increases the decontamination requirements for the plant. During accidents, where coolant gas escapes from the primary circuit into the containment building, ^{110}Ag can be transported to operating personnel and to the general public.

2.4.1 ^{110}Ag release under normal event conditions

During the first operation phase, ^{110}Ag produced in the fuel kernels is released to a large extent into the particle coating and stored there [Ve01]. Only a small fraction, in the order of 1% to 3%, of silver produced passes the coating and the compact matrix and is released into the coolant. In the beginning of the high- temperature phase, the release of silver from the fuel compact significantly increases as a result of an enhanced diffusive transport through the silicon carbide barrier coating layer. The respective diffusion coefficient (at 1 290 °C) is higher by a factor of 10 compared with the low- temperature level (at 827 °C). In contrast, the increase of the diffusion coefficients in the kernel and pyrolytic layer is less pronounced. The release from the compact is stronger than the steady silver production in the kernel, so much so that the amount of ^{110}Ag remaining in the kernel decreases. As soon as the fuel temperature decreases to its lower level, continuously produced silver is predominantly stored in the coating again, while release into the coolant is significantly reduced.

2.4.2 ^{110}Ag release under abnormal event conditions

^{110}Ag is released from spherical fuel elements under accident conditions [Me04]. Typical accident conditions include loss of forced coolant either from large or from small breaks. For the current PBMR design, the core heats up due to radioactive decay of ^{110}Ag contained in the fuel sphere. The helium gas volume in the core expands due to increased temperatures at constant pressure, whereby ^{110}Ag is transported from the core cavern into the depressurised main power system circuit. After approximately 36 hours, the maximum average core temperature is reached and the gas expansion reverses. Thus, after 36 hours, no more ^{110}Ag is released from the core cavern than may have been released from the fuel spheres.

2.4.3 The decay of ^{110}Ag

^{110}Ag decays (98.3%) via seven β branches to excited levels of ^{110}Cd [Fu58]. The subsequent decays comprise more than 50 γ transitions. There is also a 1.14% branch that de- excites by γ emission to ^{110}Ag, which further decays (95.2%) with a half life of 24.5 seconds, by β emission of 2 893 keV, to the ground state of ^{110}Cd. These decay branches are shown in Equations 2.2 and 2.3.

$$^{110}Ag \xrightarrow{98.3\%} {}^{110}Cd + \beta^- \qquad 2.2$$

$$^{110}Ag \xrightarrow{1.14\%} {}^{110}Ag + \gamma \xrightarrow{95.2\%} {}^{110}Cd + \beta^- \qquad 2.3$$

The radioactive nuclide ^{110}Ag has a complex decay scheme, as shown schematically in Figure 2.2. In this figure, only the two main β branches, which constitute 98.3% of the β transitions of ^{110}Ag and γ - rays with branching ratios greater than 1%, have been included.

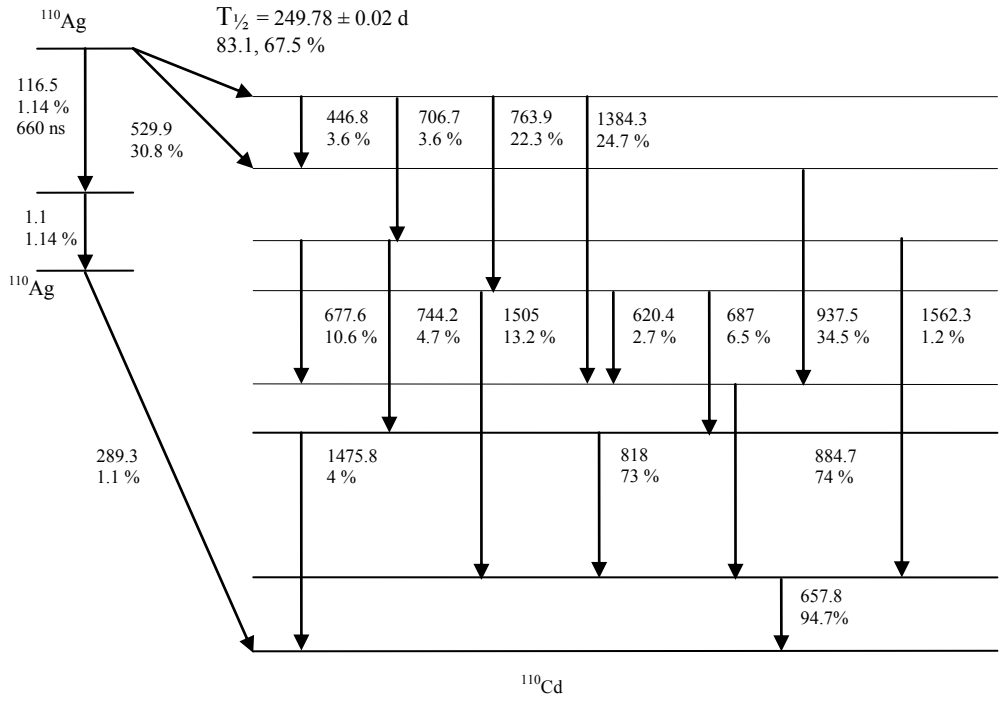

Figure 2.2: Simplified decay scheme of ^{110}Ag

2.4.4 Structure of ^{110}Ag

An atom of ^{110}Ag has 47 protons, 63 neutrons and 5 electron shells (energy levels) with a total of 47 electrons. Beginning with the shell closest to the nucleus and

working outward [Be09], a ground state electron configuration of an ^{110}Ag atom is: $1s^2$ $2s^2$ $2p^6$ $3s^2$ $3p^6$ $3d^{10}$ $4s^2$ $4p^6$ $4d^{10}$ $5s^1$ [Ko09]. Each electron has a certain orbital angular momentum with magnitude given by $\sqrt{l(l+1)}\hbar$ [Ei85]. The value of l depends on which orbital the electron is located in. l is 0 for orbital s, 1 for orbital p, 2 for orbital d, 3 for orbital f, 4 for orbital g and so on, alphabetically. This means that any electron in orbital s has zero orbital angular momentum. All electrons have intrinsic angular momentum (the angular momentum as a result of the rotational motion about their axis) of the same magnitude but different direction ±ħ/2, depending on where the electron is located in the orbit. Figure 2.3 shows the structure of a Ag- atom and table 2.1 shows the properties of silver. The temperature at which silver vaporises is proportional to the pressure, as shown in table 2.2.

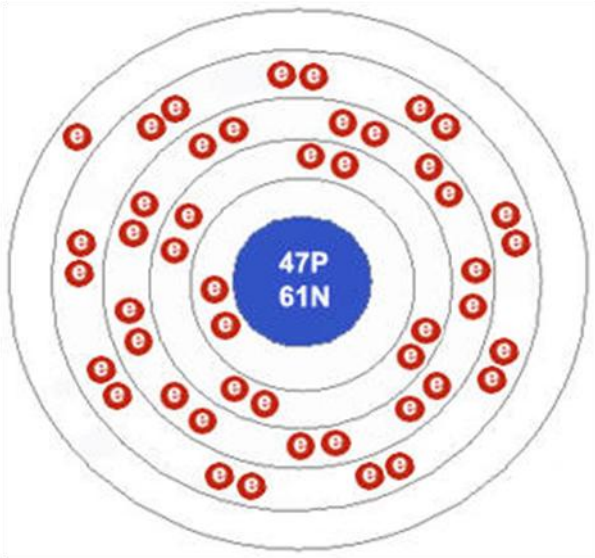

Figure 2.3: Structure of Ag-atom [Be09]

Table 2.1: Properties of silver [Be09]

Atomization	284 kJ/mol
Boiling point	2 211 °C
Density at 20 °C	10.5×10^{19} g/cm^3
Mass magnetic susceptibility	-2.27×10^{-9}
Electrical resistivity	1.59×10^{-6} Ω /cm
Melting point	961.93 °C
Molar volume	10.335 cm^3/mol
Vaporisation thermal conductivity	42.9 W/m/K
Vaporisation	257.7 kJ/mol

Table 2.2: Vaporisation temperature of silver as a function of pressure [Li99]

Pressure, P (mbar)	Temperature at which silver vaporises, T (°C)
10^{-5}	995.57
10^{-4}	995.7
10^{-3}	997
10^{-2}	1010
10^{-1}	1140

2.5 Stern-Gerlach experiment

After the discovery (in 1896) of the Zeeman effect, its theoretical interpretation confirmed that atoms have magnetic dipole moments. The question remained as to whether space quantization really occurs; that is, whether the projections of the angular momentum and its associated magnetic moment on an axis defined by the direction of an imposed magnetic field are quantized (equal to an integral multiple of $\hbar$, where $\hbar = h/2\pi$ and h is a Planck's constant). For example, whether the projection of the intrinsic angular momentum m_s of the valance electron of a silver atom can be only one of the two values, $-eh/2m$ or $eh/2m$ instead of being any value in the interval $[-eh/2m,\ eh/2m]$. As a result, the associated magnetic moment can be only one of the two values, $-eh/2m$ and $eh/2m$ as the magnetic moment is equal to $2m_s\, eh/2m$. This would make the atoms in a beam of silver atoms split into two, corresponding to the deflecting force that is proportional to $-eh/2m$ or $eh/2m$.

In 1921, Otto Stern proposed an experiment to answer this question. It consisted of generating a beam of Ag- atoms from a crucible, passing it through an inhomogeneous magnetic field and observing how the beam was deflected by the force exerted by the field on the magnetic dipole moments of the atoms. The detector was a glass plate on which the Ag- atoms in the deflected beam would be deposited. The schematic layout of the experimental setup is shown in figure 2.4. The experiment took place in vacuum in order to avoid the collision of atoms. Ag- atoms leaving the crucible would travel in different directions, and if they were allowed to reach the magnetic field with such a motion, it would be difficult to detect their deflection on the glass plate. As a result, a beam of Ag- atoms was collimated with a pair of slits (0.03 mm wide), as shown in figure 2.4, in order to observe clearly the separation of a beam on the glass plate after it passed through the inhomogeneous magnetic field. The deflecting force that acted on the silver atoms is given by $F_z = \mu_z \frac{\partial B_z}{\partial z}$, where μ_z is the magnetic dipole moment of a Ag- atom in the z- direction and $\frac{\partial B_z}{\partial z}$ is the gradient of the magnetic field in the z-direction [Be08]. The magnetic dipole moment is given by $\mu_z = \pm eh/2m$, where e is the

charge of the electron, h is Plank's constant 6.62×10^{-34} Js, z is the direction of the magnetic field and m is the mass of the electron.

The distribution of deflections would decrease monotonically on either side of zero-deflection, if the magnetic moments were randomly oriented, reflecting a random distribution of the dipole orientations. The beam should be split into two distinct beams corresponding to the parallel and anti- parallel alignments of the magnetic moments with respect to the direction of the inhomogeneous magnetic field [De85]. This is due to the fact that the distance of deflection of Ag- atoms is proportional to the magnetic moment of the valence electron. As a result, the distribution of deflections of Ag- atoms would be the same as the distribution of the dipole orientations. For example, if the dipole orientations had a uniform distribution, then the distribution of the deflection of silver atoms would also be uniform. The spot observed on the target plate of the beam of Ag- atoms, after passing the region of magnetic field, would have a uniform distribution. Figure 2.4 shows the predicted distribution of the beam of Ag- atoms on the target plate after passing through the inhomogeneous magnetic field for the non- random and random distribution of dipole orientations.

Stern was clumsy with his hands and never touched the apparatus of his experiments. He enlisted Walther Gerlach, a skilled experimentalist, to collaborate in the experiment. Stern predicted that the effect would be just barely observable. They had difficulty in raising support in the midst of the post World War I financial turmoil in Germany. The apparatus, which required extremely precise alignment and a high vacuum, kept breaking down. Finally, after a year of struggling, they obtained an exposure of sufficient length to give promise of an observable silver spot on the glass target plate. At first, when they examined the glass plate they did not see anything. Then, gradually, the spot of Ag- atoms became visible, showing a beam separation of 0.2 mm [Fr03]. Apparently, Stern could only afford cheap cigars with high sulphur content. As he puffed on the glass plate, sulphur fumes converted the invisible deposit of silver into visible black silver sulphide, and the splitting of the beam was observed.

The new quantum mechanics of Heisenberg, Shrödinger and Dirac (1926- 1928) showed that the orbital angular momentum of the Ag- atom in the ground state is actually zero. Its magnetic moment is associated with the intrinsic spin angular momentum of the single valence electron, the projection of which has values of $\pm \hbar/2$ consistent with the fact that the silver beam is split in two. If Stern had chosen an atom with $L = 1$, $S = 0$, then the beam would have split into three, the gap between the $m = +1$ and $m = -1$ beams would have been filled in, and no split would have been visible.

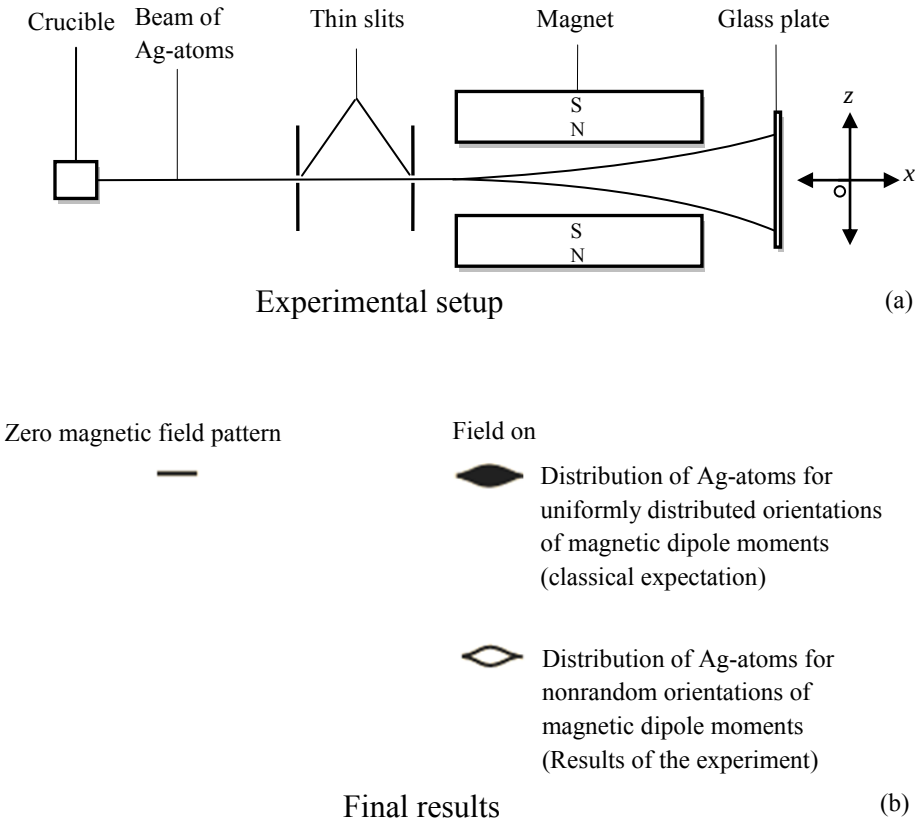

Figure 2.4: Experimental set-up (a) and final results (b) of the Stern-Gerlach experiment

3 CHAPTER 3

APPLICABLE THEORY

Theory applicable to this thesis is provided in this chapter, with specific emphasis on the following: magnetic circuit theory, the effect of an external magnetic field on the total angular momentum of an atom and the deflection of atoms.

3.1 Speed distribution of Ag- atoms

In order to produce a beam of Ag- atoms of a specific average velocity, a crucible heated to a defined temperature T is used. In the crucible, the evaporated Ag- atoms are sufficiently numerous to acquire a Maxwellian velocity distribution. Figure 3.1 shows the speed distribution of the atoms for $T_1 < T_2 < T_3$. According to the Maxwell-Boltzmann distribution, the fraction of atoms with the speed between v and dv evaporating from the surface is given by:

$$f(v)dv = \frac{4}{\sqrt{4\pi}}\left(\frac{v}{v_{mp}}\right)^2 Exp\left(-\left(\frac{v}{v_{mp}}\right)^2\right) d\left(\frac{v}{v_{mp}}\right)$$

where

$v_{mp} = \sqrt{\frac{2kT}{m}}$ is the most probable (mp) speed of the atoms

k = 1.38066 x 10^{-23} J/K is the Boltzmann constant

m is the mass of an atom, kg

T is the temperature within the crucible, K

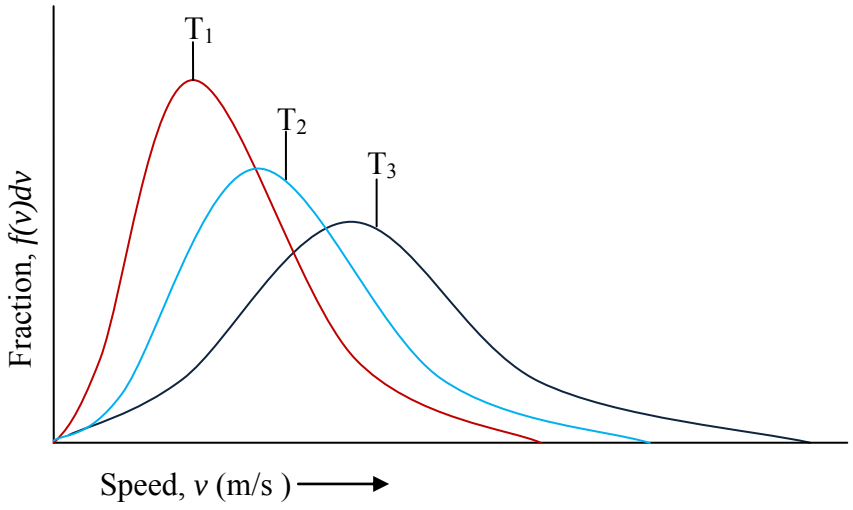

Figure 3.1: Velocity distribution of atoms

Ag- atoms from the crucible are emitted isotropically and it is possible to observe their deflection on the glass plate. A beam of Ag- atoms was collimated with a pair of collimators in order to observe the deflection of the beam with a given direction on the glass plate after having passed through a magnetic field.

3.2 Magnetic circuit with gap

From Ampere's law for a magnetic circuit containing a gap as shown in figure 3.2 [Sy97], the length of the gap l_g can be found using the relationship

$$H_d l_m = H_g l_g + V_{mi} \tag{3.1}$$

where

H_d is the magnetic field intensity of the magnet, [A.m^{-1}]
l_m is the length of the magnet, [m]
H_g is the magnetic field intensity in the gap, [A.m^{-1}]
l_g is the length of the gap, [m]
V_{mi} is the reluctance drop in the other ferromagnetic portion, [kg^{1}.m^{-1}.s^{2}.A^{2}].

The cross-sectional area of the magnet can be found from the flux required in the gap using the relationship

$$B_d A_m = K B_g A_g \tag{3.2}$$

where

B_d is the flux density in the magnet, [T]
A_m is the cross-sectional area of the magnet $l_m \times c$, [m^2]
B_g is the flux density in the gap $l_m \times c$, [T]
A_g is the cross-sectional area of the gap, [m^2]
K is a dimensionless leakage factor

A leakage factor for the configuration of figure 3.2 is given by [Sy97]

$$K = 1 + \frac{l_g}{A_g} 0.67 C_a \left[1.7 \left(\frac{0.67 C_a}{0.67a + l_g} \right) + \frac{l_g}{2a} \right] \tag{3.3}$$

where

$C_a = 2A_m$
a is a portion of a magnetic circuit shown in figure 3.2

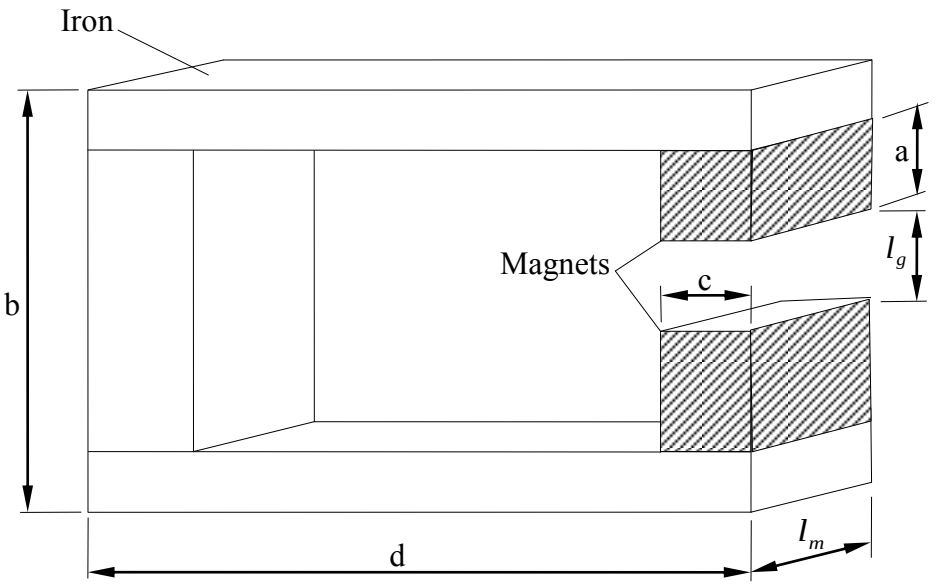

Figure 3.2 Magnetic circuit with gap l_g.

3.3 Effect of an external magnetic field on the total angular momentum of a Ag- atom

According to classical mechanics, it can be shown that an electron in a circular orbit, as illustrated in figure 3.3**,** has an angular momentum $\vec{L} = mr^2\omega$ and an associated magnetic moment $\mu = (e/2m)\vec{L}$, where m and e are the mass and charge of the electron, and r and ω are the radius and angular velocity of the orbital motion [Fl99]. In a magnetic field $\vec{B}$ the atom will be acted on by a torque $\tau = \vec{\mu} \times \vec{B}$, due to the interaction of its magnetic moment $\vec{\mu}$ and the magnetic field. This torque causes $\vec{L}$ to process about the direction of $\vec{B}$. The torque will be maximum when $\vec{\mu}$ and $\vec{B}$ are perpendicular and zero if they are parallel. The atom will also have a potential energy $U = -\mu \bullet B$. If the field is inhomogeneous such that at a certain point it is in the z direction and varies strongly with z, then the atom will be acted on by a force $F_z = \pm\mu_z \frac{\partial B_z}{\partial z}$ such that F_z can have any real value in the interval $\left[-\mu \frac{\partial B_z}{\partial z}, \mu \frac{\partial B_z}{\partial z} \right]$. A monoenergetic beam of atoms, initially randomly oriented and passing through an inhomogeneous magnetic field, would be expected to be deflected in the +z and -z directions with a distribution of deflection angles that has a maximum value at zero deflection and decreases monotonically in either direction. However, this is not what is observed. Instead, an atomic beam, passing through such a field, is generally split into several distinct beams, implying that the sideways force deflecting the beam is restricted to certain discrete values.

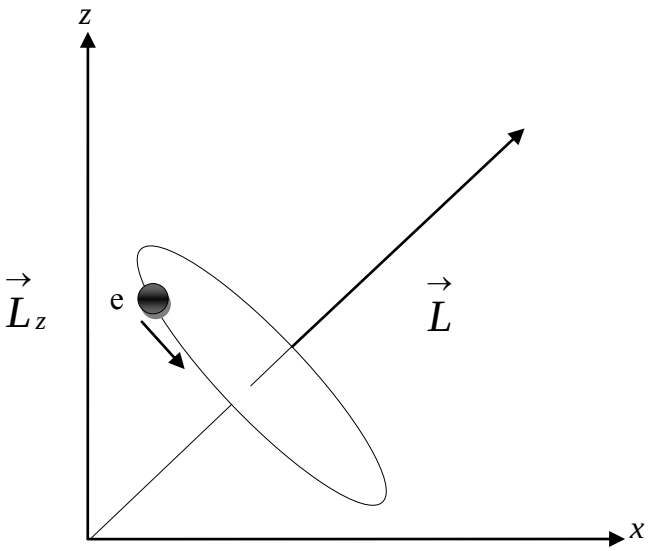

Figure 3.3 Illustration of the angular momentum vector.

According to quantum mechanics, an atom can exist in a steady state (an eigenstate of the Hamiltonian) with a definite value of the square of the magnitude of its total angular momentum, $\vec{F}\bullet\vec{F}$ and a definite component F_z of its angular momentum in any particular direction, such as that of the z axis [Fe61]. Moreover, these quantities can only have discrete values specified by the equations $\vec{F}\bullet\vec{F} = f(f+1)h^2$ and $F_z = m_f\hbar$ where f is the angular momentum quantum number, and can only be integer or half integer; m_f is the magnetic quantum number and can have only the values: $[-f, -(f-1), \ldots +(f-1), f]$ and $\hbar = h/2\pi$. The magnetic moment associated with the angular momentum is $\vec{\mu} = (ge/2m)\vec{F}$ where the gyromagnetic factor g is the characteristic of the atomic state and is in the order of unity. The projection of μ on the z axis can have only one or another of a discrete set of values $\mu_z = gm_f\mu_B$, where μ_B = 9.270154x10^{-24} J/T is the *Bohr magneton*. In the presence of an inhomogeneous magnetic field in the z direction, the atoms will be acted on by a force that can have only one or another of a discrete set of values $m_f g\mu_B \frac{\partial B}{\partial z}$. When a monoenergetic beam of such atoms, distributed at random among states with $2f+1$ possible values of m_f, passes through an inhomogeneous magnetic field, it is split into $2f+1$ beams. These beams are deflected into $\pm\mu$ directions with deflection angles corresponding to the various possible discrete values of the force. Thus, if a beam of atoms of some particular species were observed to be split into, six beams, for example, then one could conclude that the angular momentum quantum

number associated with the magnetic moment responsible for the deflection is (6-1)/2 = 5/2.

Turning now to the present experiment in which a beam of Ag- atoms passes through an inhomogeneous field: It should be first noted that the total angular momentum is the sum of the spin and orbital momenta of the electrons and nucleons. The electronic ground state of a Ag- atom is the S- state, which means that the total orbital angular momentum of the electrons L is equal to 0 (the atom is in an S- state). One unpaired electron has an intrinsic spin being equal to 1/2 and the total angular momentum is $\vec{J} = \vec{L} + \vec{S} = \hbar/2$. The magnetic moment associated with the spin of the electron is $g_s \mu_B \vec{S}/\hbar$, where $\vec{S}$ is the spin angular momentum and g_S = 2.002319304 is the gyromagnetic ratio of the electron. The nuclear angular momentum (total spin and orbital momenta of the nucleons) of ^{109}Ag, the isotope of silver used in this study, is $I = \hbar/2$. The nuclear magnetic moment is $g_n \mu_B \vec{S}/\hbar$, where g_n is much smaller than $m_e/m_p \approx 1/1386$.

In magnetic field free space, the interaction between the magnetic moments associated with the total electronic angular momentum $\vec{\mathrm{J}} = \vec{\mathrm{L}} + \vec{\mathrm{S}}$ and nuclear angular momentum $\vec{I}$ causes them to process around their sum $\vec{F} = \vec{J} + \vec{I}$ which is the total angular momentum of the atom. According to the rules for combining angular momenta, the quantum number of the sum is $f = i \pm j = 0$ or 1. With each combination there is an associated magnetic moment of which the value can be calculated by matrix mechanics or, more simply, by the 'vector' model. Ag- atoms emerging into a field-free region from the crucible at temperature of ~1 000 °C will be

i. almost exclusively in the ground electronic state;
ii. nearly equally distributed among the two hyperfine states with f = 0 and $f = 1$; and
iii. very nearly equally distributed among the degenerate 'magnetic' substates of each of the hyperfine states (states with the same f but different m_f, where the latter is the quantum number of the component of total angular momentum in the direction of the field).

A well- focused beam of such atoms passing through a weak inhomogeneous field would be split into as many beams as there are magnetic substates with different components of magnetic moment in the direction of the field. A weak field is an external field in which the torque exerted by the field on the magnetic moments associated with either I and J are small compared to the torque on each that results from the mutual interaction of their magnetic moments. In a strong inhomogeneous field, $\vec{I}$ and $\vec{J}$ are 'decoupled' and both process independently about the external field direction. The magnetic moment of the Ag- atom is then dominated by the magnetic moment associated with the decoupled $\vec{J} = \vec{S}$, of which the projection on the direction of the external field can have only the values $\mu_z = \pm g_S \mu_B/\hbar$. The beam is thus split

into two groups of components, with each group having a 'hyperfine' splitting due to the nuclear spin, which can only be resolved by very refined atomic beam techniques such as the polarised proton source at iThemba LABS.

3.4 Deflecting force acting on Ag- atoms

In this experiment, a beam of neutral Ag- atoms with direction *x* was directed through a strong inhomogeneous magnetic field gradient transverse to the beam. The field exerts a deflecting force on the magnetic dipole moments of moving atoms. If the magnetic field gradient is taken to be in the *z*- direction, then the *z*- component of the force [Fr09] is given by

$$F_z = \mu_z \frac{\partial B_z}{\partial z} \qquad 3.4$$

where

$\frac{\partial B_z}{\partial z}$, [T/m] is the gradient of the magnetic field in the *z*- direction and

μ_z = 9.270154x10^{-24} J/T.

3.5 The distance of deflection *z* of Ag- atoms

Figure 3.4 shows the paths of Ag- atoms with opposite spins. The central axis of the beam is taken as the *x* axis and the magnetic field direction as the *z* axis, as illustrated in figure 3.4. To calculate a distance of deflection for the atom of mass *m* and velocity *v,* it is assumed that the deflecting force is constant in the region between the pole pieces traversed by the beam, and zero elsewhere. If *z* is the distance of deflection of an atom due to the force F_z exerted during its passage between the pole pieces, *z* is then given by the solution for Newton's second law with constant acceleration:

$$z = \frac{v_z t_m}{2} + v_z t_{mg} \qquad 3.5$$

where

$$v_z = \frac{F_z}{m} t_m,\ t_m = \frac{l_m}{v_x},\ t_{mg} = \frac{l_{mg}}{v_x}$$

l_m is the magnet length, [m]

l_{mg} is the distance from the edge of the magnet to the target plate, [m]

Because the angle of deflection of the beam is small, it follows that v_x can be approximated by $v = |\bar{v}|$ .The expression for the deflection is then given by

$$z = F_z l_m \left(\frac{l_{mg} + \frac{l_m}{2}}{mv^2} \right) \qquad 3.6$$

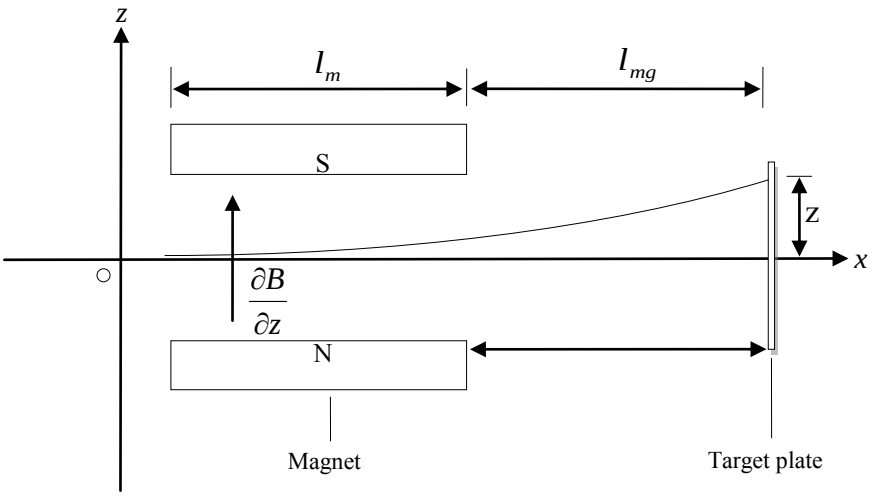

Figure 3.4: Path of a Ag-atom under the influence of an inhomogeneous magnetic field

4 CHAPTER 4

EXPERIMENTAL WORK

An apparatus was constructed and used to deflect the Ag- atoms in both homogeneous and inhomogeneous magnetic fields. The schematic layout of the apparatus is shown in figure 4.1 and a photograph of the complete experimental set- up is shown in figure 4.2. Figures 4.3 and 4.4 show the photographs of the vacuum chamber with and without the magnetic circuit inside. A beam of Ag- atoms was generated in the crucible by vaporising silver grains (99.9% pure) in a vacuum of ~10^{-5} mbar. The silver beam was collimated by a pair of thin collimators through the gap of a magnetic circuit, where it experiences a magnetic field. Due to the interaction of atomic spin and magnetic field, the beam of Ag- atoms is deflected onto a target plate.

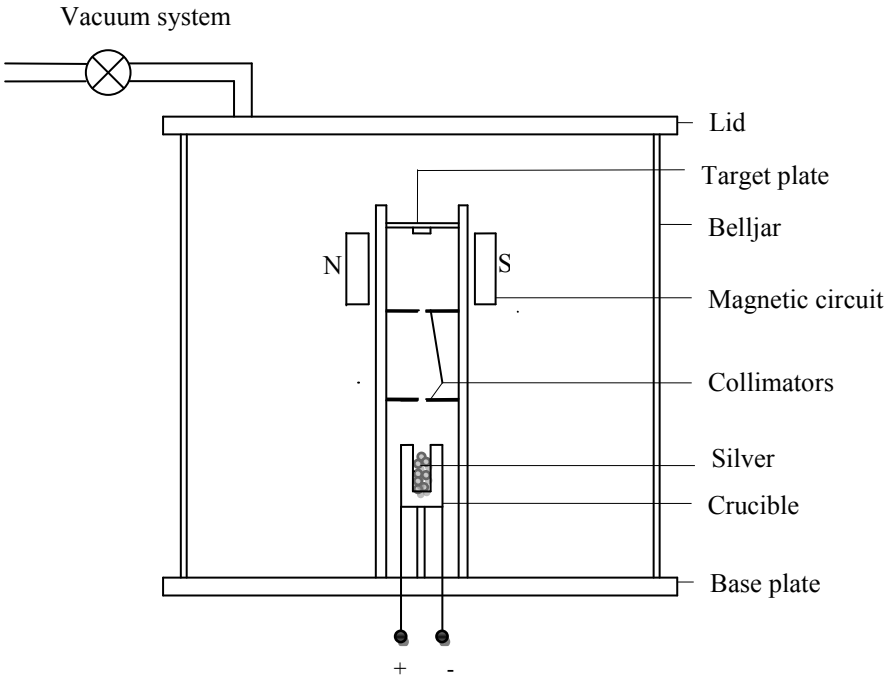

Figure 4.1: Schematic layout of the experimental set- up

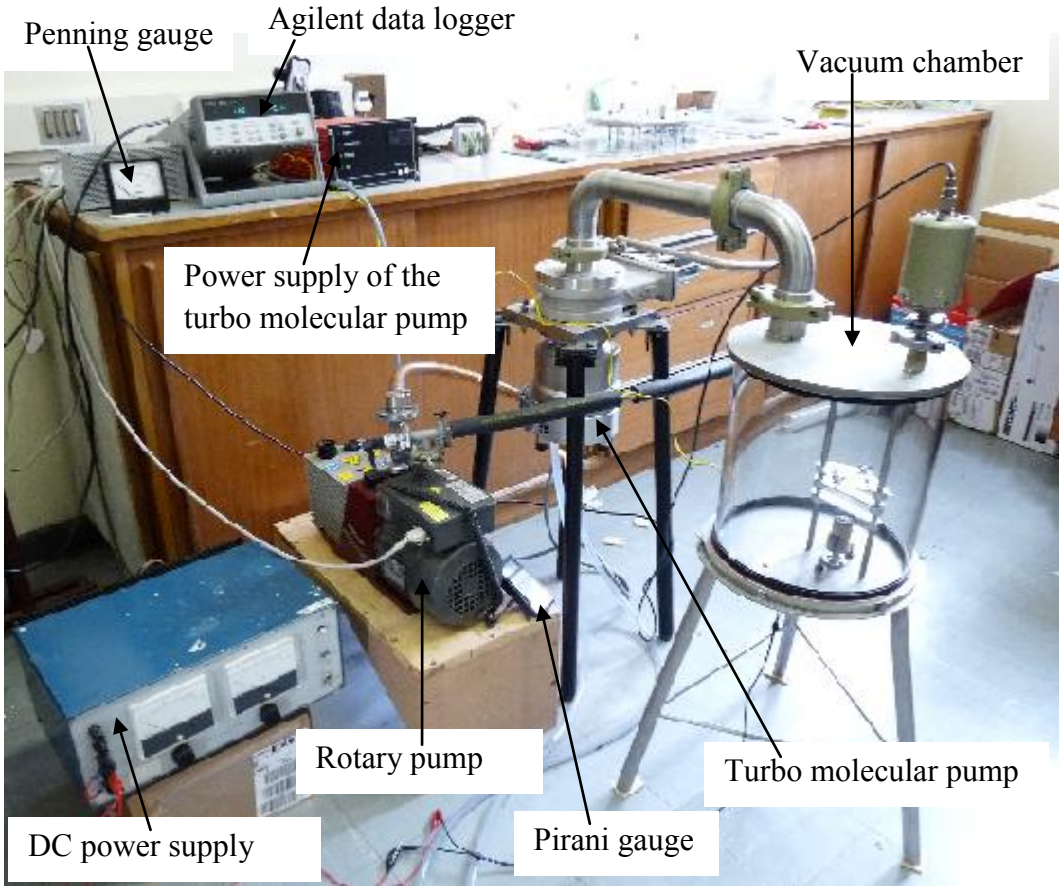

Figure 4.2: Photograph of the complete experimental set-up

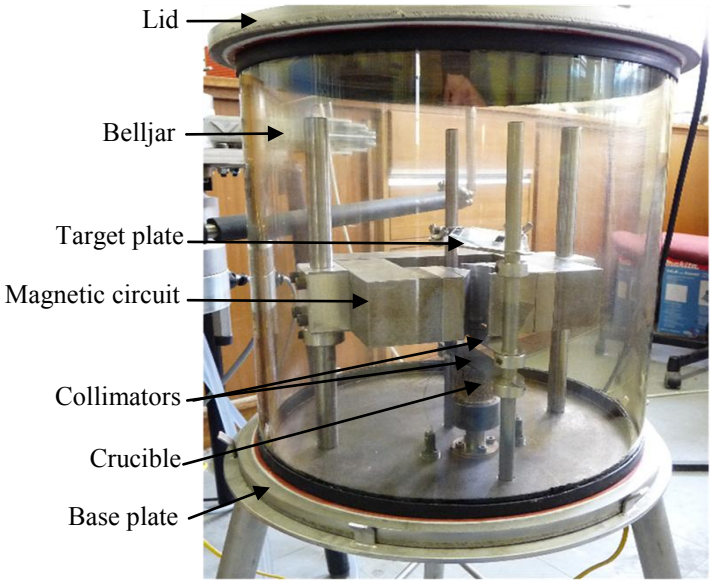

Figure 4.3: Photograph of the experimental set- up within the vacuum chamber

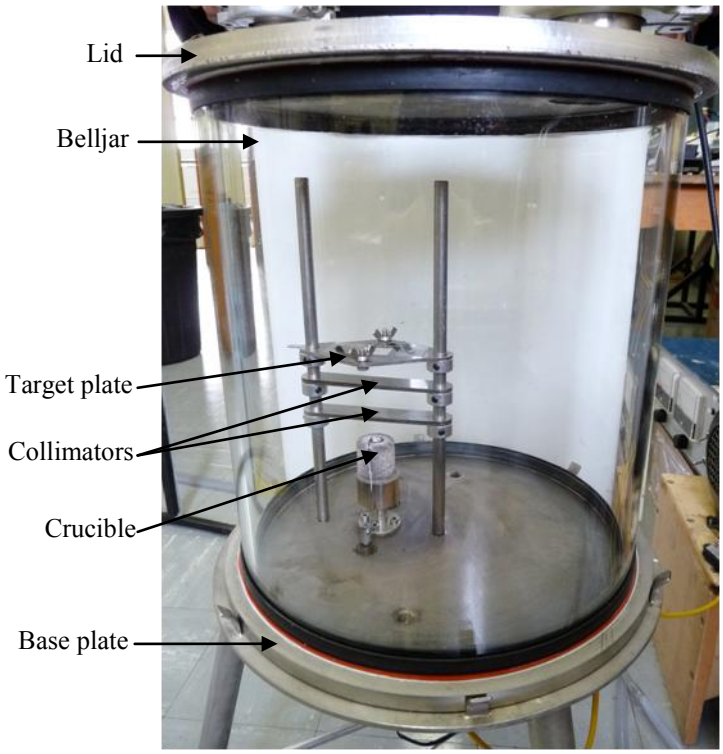

Figure 4.4: Photograph of the vacuum chamber without a magnetic circuit inside

4.1 Experimental set-up

The apparatus consists of a number of components as shown in figure 4.2. In this section a detailed description of the components is given. Photographs and schematic layouts of the components displayed in figure 4.2 are also provided.

4.1.1 Target plate

The target plate used was a rectangular glass slide mounted onto the holder. Figure 4.5 shows a schematic layout of the target plate fixed on its holder. The holder was a stainless steel plate of 1.5 mm thickness, with two holes on two opposite sides. These two holes act as guides for the target plate to slide up and down. They were the reference points to ensure that the target plate stayed aligned with the crucible.

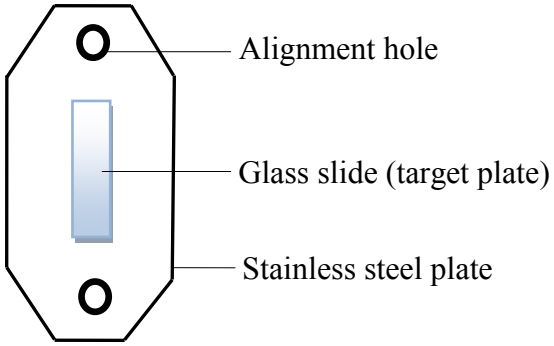

Figure 4.5: Schematic layout of the target plate and its holder

4.1.2 Vacuum system

The vacuum chamber was made up of a belljar with a diameter of 281 mm and a height of 314 mm, and two aluminium plates. The aluminium plates formed the base and cap of the vacuum chamber and were sealed at the glass by a flat silicon rubber seal. The experiments were run in vacuum at ~10^{-5} mbar, as this allows Ag- atoms to move without colliding with air molecules. This pressure was achieved by using two vacuum pumps, a rotary and a turbo molecular pump. The rotary pump draws the pressure down to 10^{-2} mbar and the turbo molecular pump from 10^{-2} to 10^{-5} mbar. The pressure was measured by two gauges, a Pirani gauge for fore vacuum measurement and a Penning gauge for high vacuum measurement. The vacuum pressure of the system was maintained by continuous pumping.

4.1.3 Collimators

Two kinds of collimators were used in this study, namely a pair of round- hole collimators and a pair of slits. The diameter of the round- hole collimators was 1 mm and the width of the slits was 0.5 mm. The collimators were made of thin stainless steel plates, 2 mm thick. The plates had two holes on opposite sides so that the height of the collimators could be adjusted. Figures 4.6 (a) and (b) show a schematic layout of the slit and round- hole collimators, respectively.

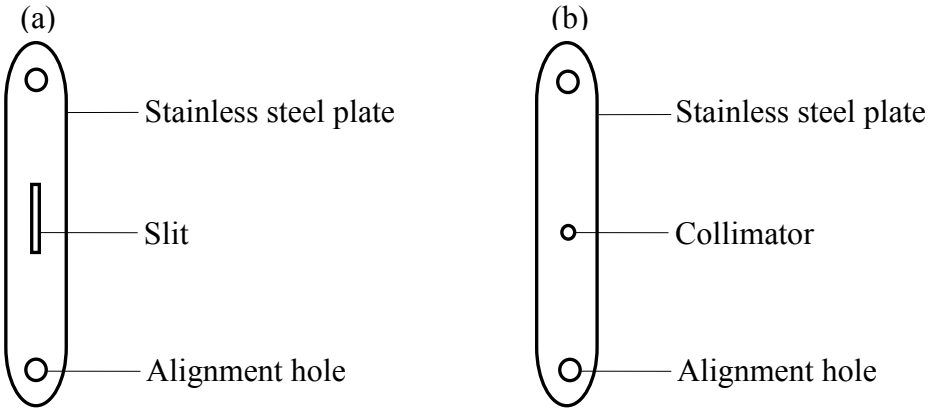

Figure 4.6: Schematic layouts of the collimators

4.1.4 Crucible

A ceramic crucible of 25 mm in height and a 5 mm inner diameter was used to vaporise natural silver metal grains to produce a Ag- atoms beam. The tungsten wire was coiled around the crucible used for heating by means of a DC power supply. The crucible was thermally insulated with a cylindrical ceramic insulator in order to generate Ag- atoms with as low input power as possible. Temperature measurements were performed using a K- type thermocouple connected to the crucible. Figure 4.7 shows a schematic layout of the insulated crucible.

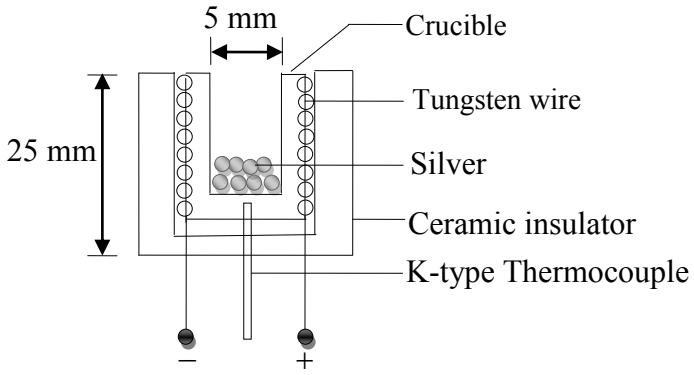

Figure 4.7: Schematic layout of the insulated crucible

4.1.5 Power supply

A 500 Watt DC power supply was used to heat the crucible. The power was kept at ~ 120 Watt.

4.1.6 Magnetic circuit

A C-shaped iron magnetic circuit was used with NdFeB permanent magnets. The design approach was based on Ampere's law [Sy97]. The aim was to design a magnetic circuit that produces an inhomogeneous magnetic field in the gap. As a result, different geometries of the magnetic circuit were examined using MagNet software [Ma09]. The geometry that best satisfied the requirements of this study is shown in Figure 4.8. The magnets are labeled in Figure 4.8, where the magnetic field lines are presented in the iron and the gap. The length of the gap and both minimum and maximum values of the magnetic flux density B (B_{min} *and* B_{max}) in the gap are also given. Point k represents the position of the beam in the gap which is 7.2 mm away from the point of maximum magnetic field B_{max}. All the other examined magnetic field geometries are shown in Appendix B.

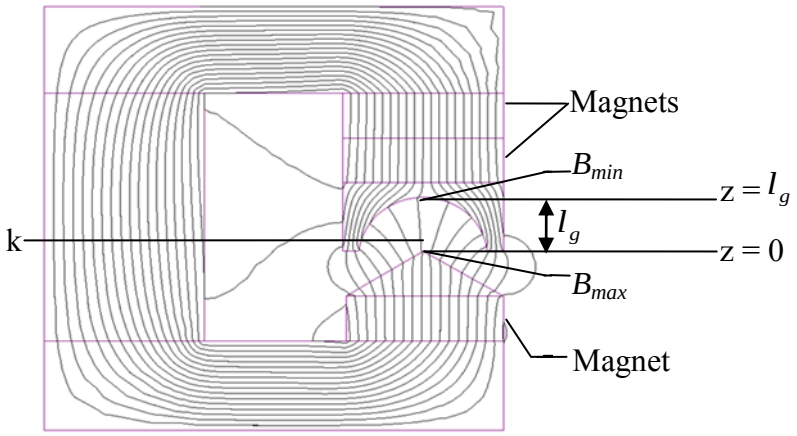

Figure 4.8: Soft iron magnetic circuit used in this study l_g = 18 mm, B_{max} = 1.04 T and B_{min} = 0.24 T

Figure 4.9 and table 4.1 show the flux density in the gap of the magnetic circuit as a function of the position z, the vertical axis as discussed in figures 3.2 and 3.4 in chapter 3. The position z ranges between 0 and 18 mm, where 0 refers to the point of maximum magnetic field, B_{max}, and 18 mm refers to the point of minimum magnetic field B_{min}. The results obtained from the MagNet software are shown in figure 4.9 while the results that were measured by a Tesla meter are shown in table 4.1 I can be noticed from figure 4.10 that the software results showed a good agreement with the measured results. To calculate a deflection of the Ag- atoms in the inhomogeneous magnetic field, the gradient of the magnetic field at the position of the beam had to be calculated. As a result, a 4^{th} degree polynomial was fitted on a measured flux density as shown in figure 4.10. The aim was to be able to calculate magnetic flied gradient using measured values of a magnetic field. It can be noticed that the polynomial made a good fit on the measured values as it gave a value of R^2 equals to 1.

Table 4.1 Flux density in the gap of the magnetic circuit that was measured by a Tesla meter

Position, Z (mm)	Flux, B (T)
0	0.9
5	0.47
10	0.38
15	0.32
18	0.27

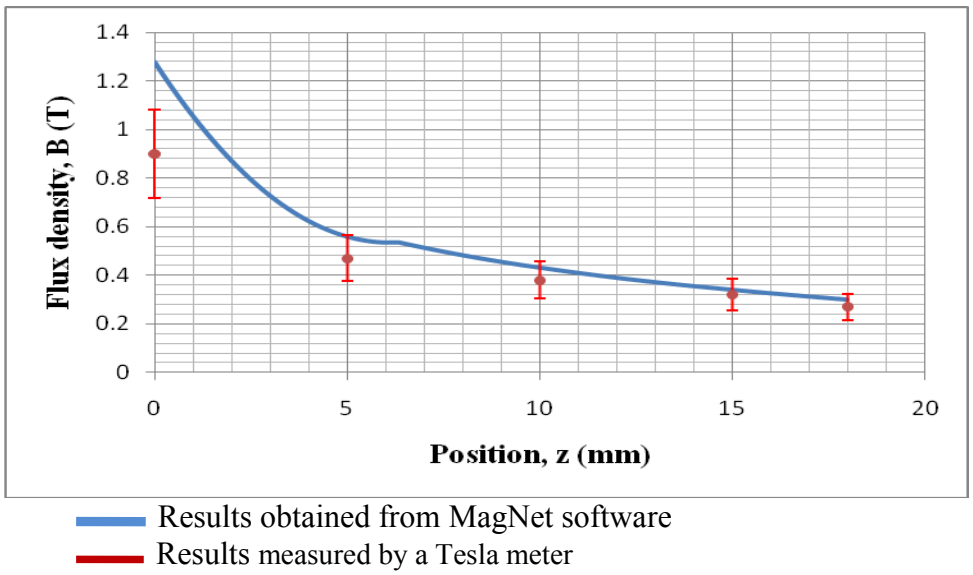

Figure 4.9: Flux density in the gap of the magnetic circuit

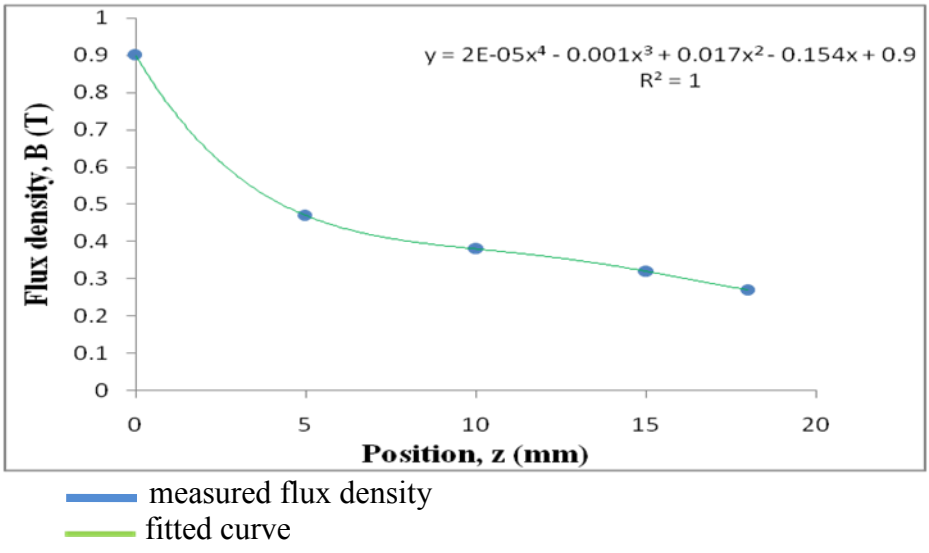

Figure 4.10: The curve fitted on a measured flux density

4.2 Operating procedure

The steps that should be followed in order to run the experiment are sequenced as follows:

i. Assemble the apparatus:
   - Place the base plate of the vacuum chamber on its stand
   - Ensure that the target plate, magnetic circuit and all collimators are tightly fitted and record their distances from the crucible
   - Clean the target plate with acetone and fasten it on its holder
   - Place the glass cylinder of the vacuum chamber on the base plate
   - Fill the crucible with silver grains
   - Connect the rotary and the turbo molecular pump to the vacuum chamber
   - Connect a thermocouple to the crucible
   - Connect a power supply to the crucible through the terminals
   - Replace the lid of the vacuum chamber

ii. Switch on the rotary pump until a pressure of $\sim 10^{-2}$ mbar is reached

iii. Open the tap to run water for cooling the turbo molecular pump

iv. Switch on the turbo molecular pump when a pressure of $\sim 10^{-2}$ mbar is reached

v. When a pressure of $\sim 10^{-5}$ mbar is reached, switch on the power supply to the crucible

vi. Increase the current on the power supply by 2 A every 15 minutes until the temperature reading on the thermocouple reaches the required value

vii. Estimate the temperature of the silver in the crucible by recording the thermocouple measurement

viii. Allow the experiment to run for approximately 2½ hours

ix. Switch off the power supply after the exposure time.

x. Switch off the turbo molecular pump, and then roughing pump

xi. Allow the temperature reading on the thermocouple to drop to ~70 °C

5 CHAPTER 5

RESULTS

Both the theoretical and experimental results are provided in this chapter. The computer code written for the theoretical calculations is given in Appendix C.

5.1 Theoretical results

The magnitude of the gradient of the magnetic field at the position of the beam of Ag-atoms in the gap was calculated and found to be 34.86 T/m. The force of deflection F_z was also calculated and its magnitude was found to be 3.23×10^{-22} N. The calculation of a gradient was done using data showing a magnetic field as a function of distance, which was obtained using a Tesla meter (see Appendix D). The deflection of Ag- atoms was calculated as a function of some assumed values of the speed in order to assess the effect of velocity distribution originating from the evaporation of atoms. The deflection was calculated using the computer program written in Visual Basic, shown in Appendix C. Figure 5.1 shows the schematic layout of the experimental set-up within the vacuum chamber.

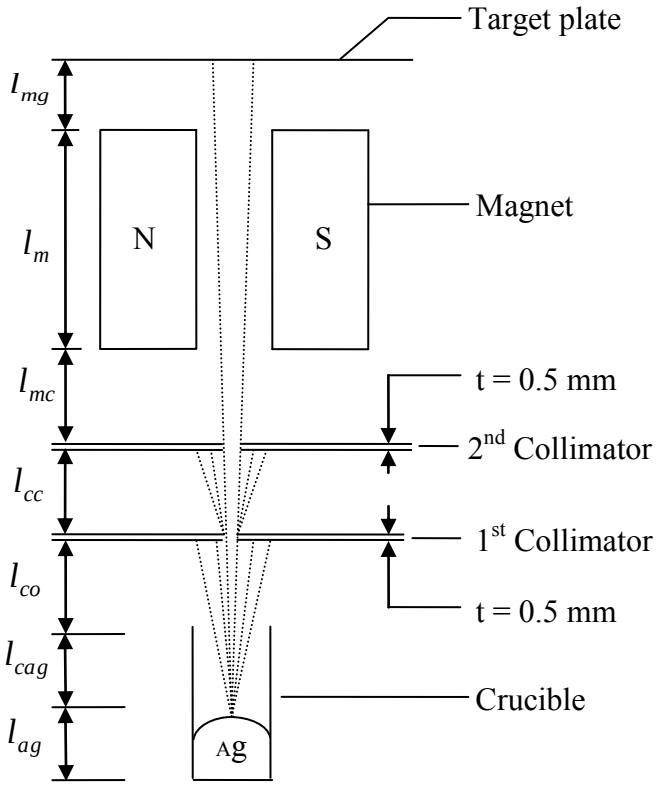

Figure 5.1: Schematic layout of the set- up within the vacuum chamber when the measurements were performed

Figure 5.2 graphically shows the results for the deflection *z* that were performed for three different lengths of magnet l_m as a function of speed *v*. These calculations were performed using the following values: l_{co} = 7.5 mm, l_{cc} = 2.5 mm, l_{mc} = 0 mm, l_{mg} = 0 mm. It was assumed that the temperature *T* of the Ag- atoms was ~1 000 °C. This figure shows that a deflection of Ag- atoms decreases as their speed increases. A comparison of

the deflections obtained at each length of magnet l_m shows that the greatest deflection is achieved at l_m = 80 mm, and decreasing the length of magnet decreases the deflection achieved.

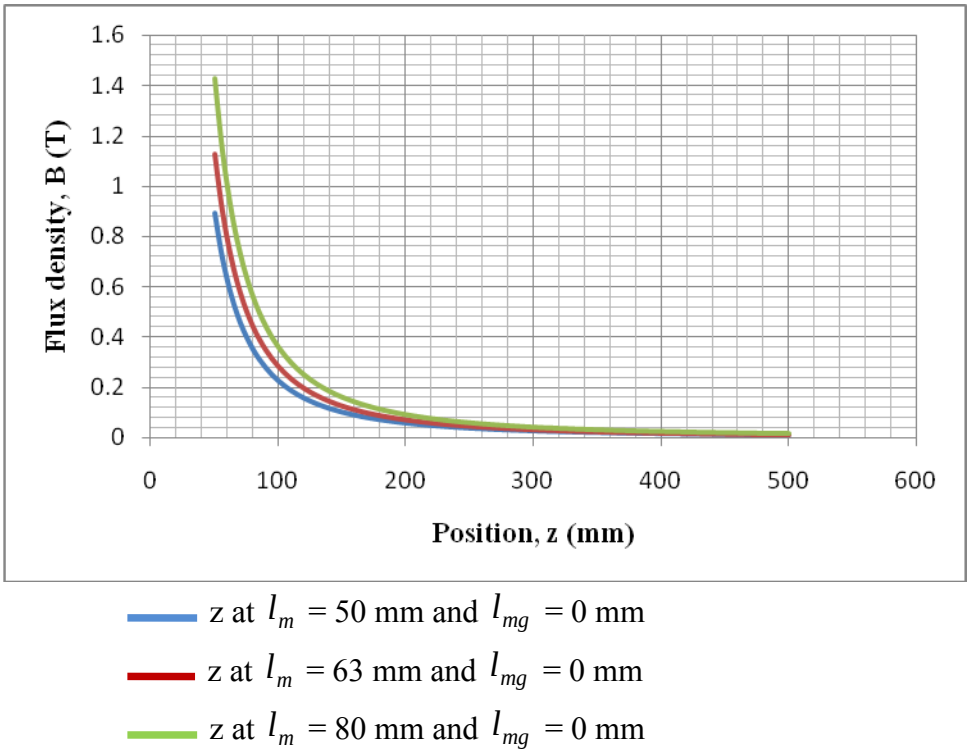

Figure 5.2: Deflection of Ag- atoms for different values of l_m

Figure 5.3 shows the results for the calculations of the deflection z of Ag- atoms that were performed for three different values of l_{mg} (distance between the target and the magnet) and as a function of the speed of the atoms *v* for each value of l_{mg}. These calculations were performed using the following values: l_{co} = 7.5 mm, l_{cc} = 2.5 mm, l_{mc} = 0 mm, l_m = 50 mm. It was assumed that the temperature *T* of the Ag- atoms was ~ 1 000 °C. This figure shows that a deviation in *z* increases with l_{mg}.

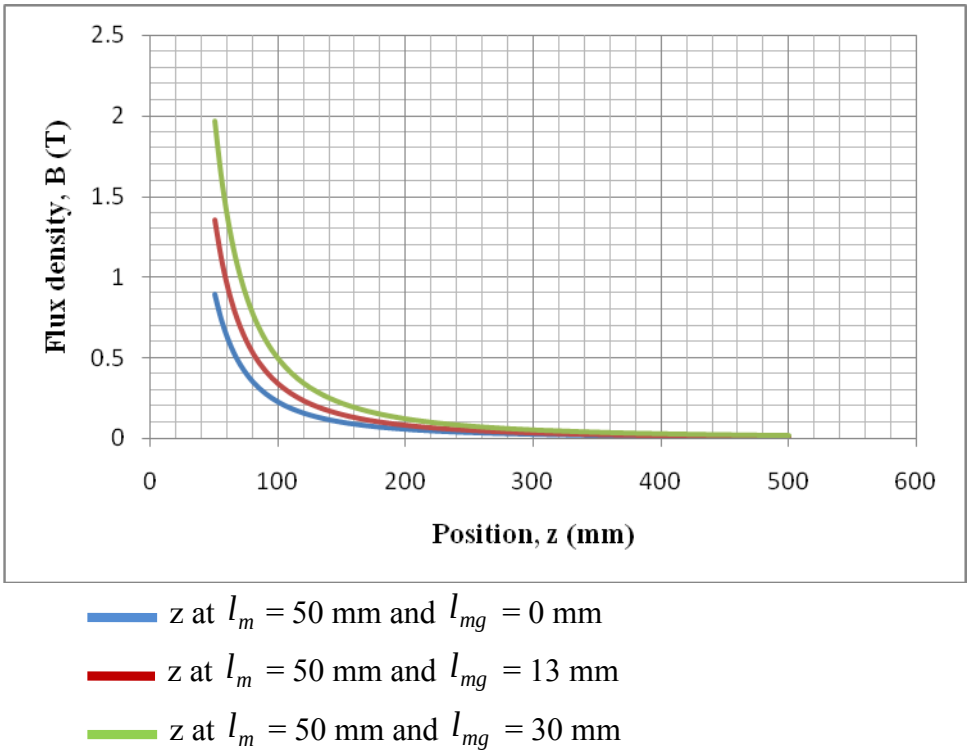

Figure 5.3: Deflection of Ag- atoms for different values of l_{mg}

5.2 Experimental results

This section illustrates the experimental results for the deflection of Ag- atoms before and after the glass slides were coated with gold. The coating of glass slides with gold was performed to enhance the silver deposits on the glass slides. It should be also noticed that the x-ray spectra of one of the samples were obtained to ensure that it was really a silver deposit. The sample was wiped with a thin weighing paper from which the spectra were obtained. The reason being the analysis of glass slides themselves was difficult as most x-rays came from the substrate itself. The corresponding results are shown in figures 5.4 and 5.5.

5.2.1 Results for deflection of Ag- atoms

The results are divided into two groups. The first group shows the deposits of silver that were observed on the glass slides of the target plate before the glass slides were coated with a thin layer of gold. The second group shows the deposits of silver that were observed after the glass slides were coated with gold. The glass slides were coated with gold to observe a clear boundary on the edge of each deposit of silver in order to measure the width of the deposit. The top rows in figures 5.6 to 5.11 are original photographs, while the bottom rows are the same photographs that have been

highlighted to show the effects noticeable on the glass slides but not clearly shown on the actual photograph. Both sets of tests were performed in the same vacuum of ~ 10^{-5} mbar and temperature of ~1 000 °C.

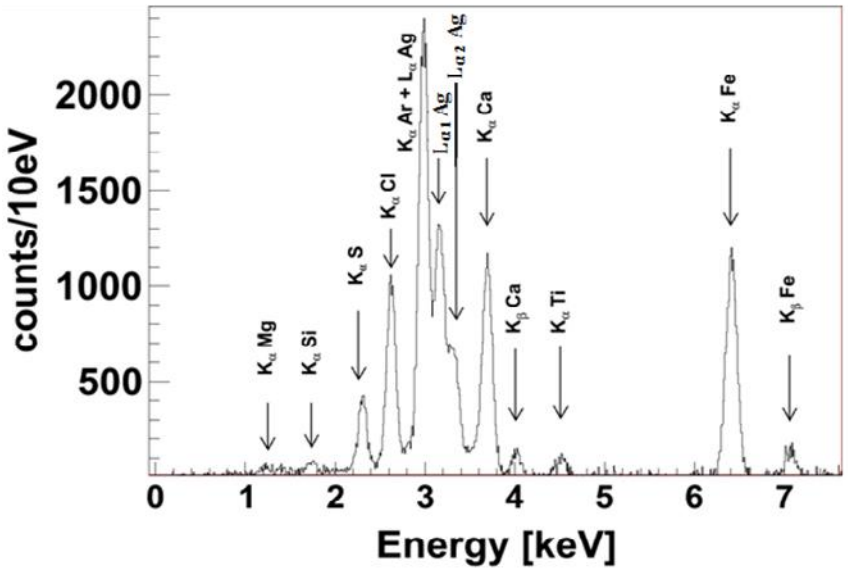

Figure 5.4 X-ray fluorescence spectrum of a glass slide in the 0 – 7 keV range

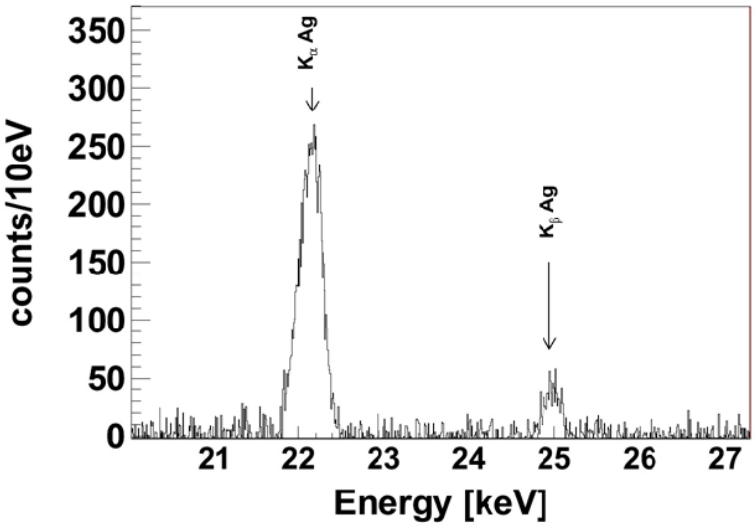

Figure 5.5 X-ray fluorescence spectrum of a glass slide in the 20 – 27 keV range

Figures 5.4 and 5.5 show X-ray fluorescence spectra obtained from the bombardment of the deposition with a 40kV Tungsten X-ray generator. The energy spectra were recorded with a XR-123 Silicon Drift Detector [amptek]. The silver deposition was collected from the glass substrate with a thin weighing paper which contains only

traces of elements with atomic number larger than 14. The content of those elements in the glass substrate overwhelms the X-ray spectrum and the characterization of the deposition was not possible otherwise.

Figures 5.4 and 5.5 are zooms on region of interest in the 0-7 keV and 20-27 keV energy range respectively. The K and L lines of Ag (see labels on the figures) clearly confirm the presence of Ag in the deposition. The spectra are background subtracted. Two spectra were recorded, one on the collected deposition and one on the paper only. It was not entirely clear whether Mg, Si, S, Cl and Ca are part of the deposition as those elements are also found on the weighing paper itself and the background was possibly not entirely subtracted because of self absorption effects and variation in the geometry between measurements. Ti and Fe are also found as trace elements and it is not entirely clear where they come from. Ar is a constituent of air in concentration of about 1% and fluoresces under X-ray irradiation. Its contribution can vary as the distance from the weighing paper to the x-ray gun and the detector can vary between two consecutive measurements. It should also be mentioned that a line from Ag is also found at the same energy as Ar but for the purpose of this measurement it was unnecessary to deconvolve.

5.2.1.1 Results before the glass slides were coated with gold

Figure 5.6 shows pictures of the spots of silver observed on uncoated glass slides. These spots were obtained with a beam collimated with a pair of round- hole collimators and the target plate positioned 13 mm away from the magnet. Figure 5.6 (a) shows the spot observed when the atoms were not acted upon by any magnetic field (the reference spot). Figure 5.6 (b) shows the spot of Ag- atoms observed when they were acted upon by the homogeneous magnetic field before they reached the target plate. This spot is slightly wider than the reference spot. Figure 5.6 (c) shows the spot of Ag- atoms that was observed when the atoms were acted upon by an inhomogeneous magnetic field before they reached the target plate. This spot is wider than both the reference spot and the spot that was obtained in the presence of the homogeneous magnetic field. It was also observed that each of these spots (figures 5.6 (a), (b) and (c)) is lighter at its edge than in the inner region.

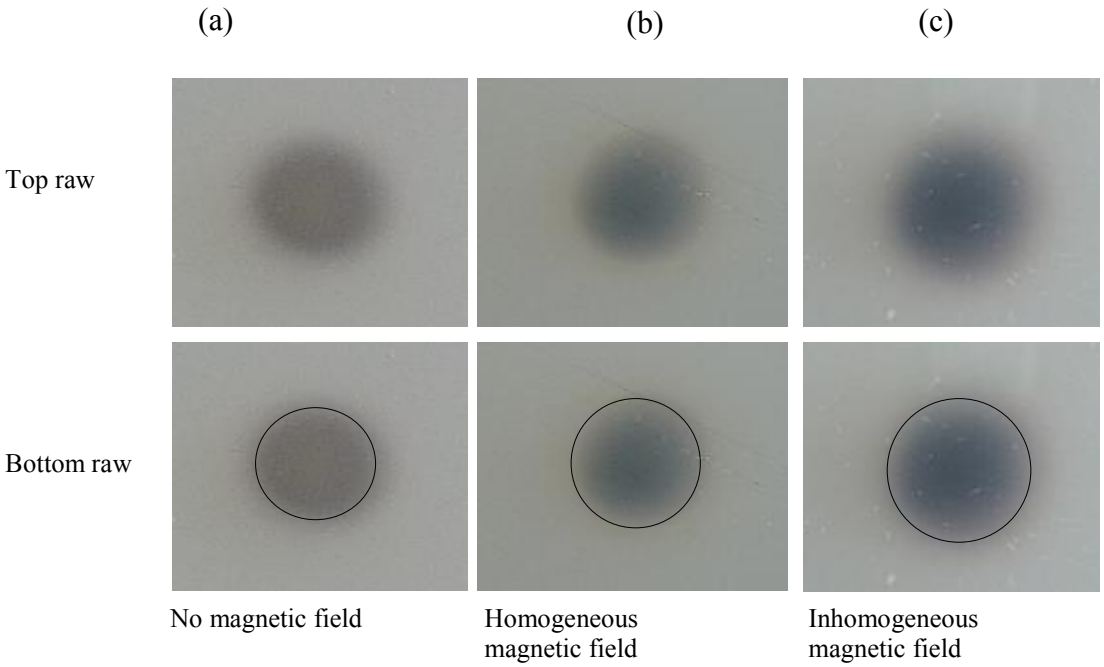

Figure 5.6: The spots of Ag- atoms at 13 mm away from the magnet

Figure 5.7 shows pictures of the spots of silver that were observed on the uncoated glass slides when the target plate was positioned 30 mm away from the magnet. The spots were observed with varying magnetic field conditions. Two of them were obtained in the presence of the magnetic field that was acting on the atoms before they reached the target plate. Figure 5.7 (a) shows the reference spot, which was observed when the atoms were not acted upon by any magnetic field. Figure 5.7 (b) shows the spot of Ag- atoms observed when they were acted upon by a homogeneous magnetic field before they reached the target plate. Again this spot is wider than the reference spot. Figure 5.7 (c) shows the spot of Ag- atoms that was observed when the atoms were acted upon by an inhomogeneous magetic field before they reached the target plate. This spot is wider than both the reference deposit and the deposit that was observed when atoms were passed through a homogeneous magnetic field. The first two spots (figures 5.7 (a) and (b)) are lighter than the spots in figures 5.6 (a) and (b). This is owing to the positioning of the target plate further from the magnet, which resulted in less intensity of the beam reaching the target plate. The last spot seen in figure 5.7 (c) is darker than the first two spots due to the increase in deposition originating from the refilling of the crucible with silver. These spots (figures 5.7 (a), (b) and (c)) are also lighter at the edge than in the inner region. Pictures of these spots and their width after the glass slides were coated with gold are shown in figure 5.10 and table 5.2.

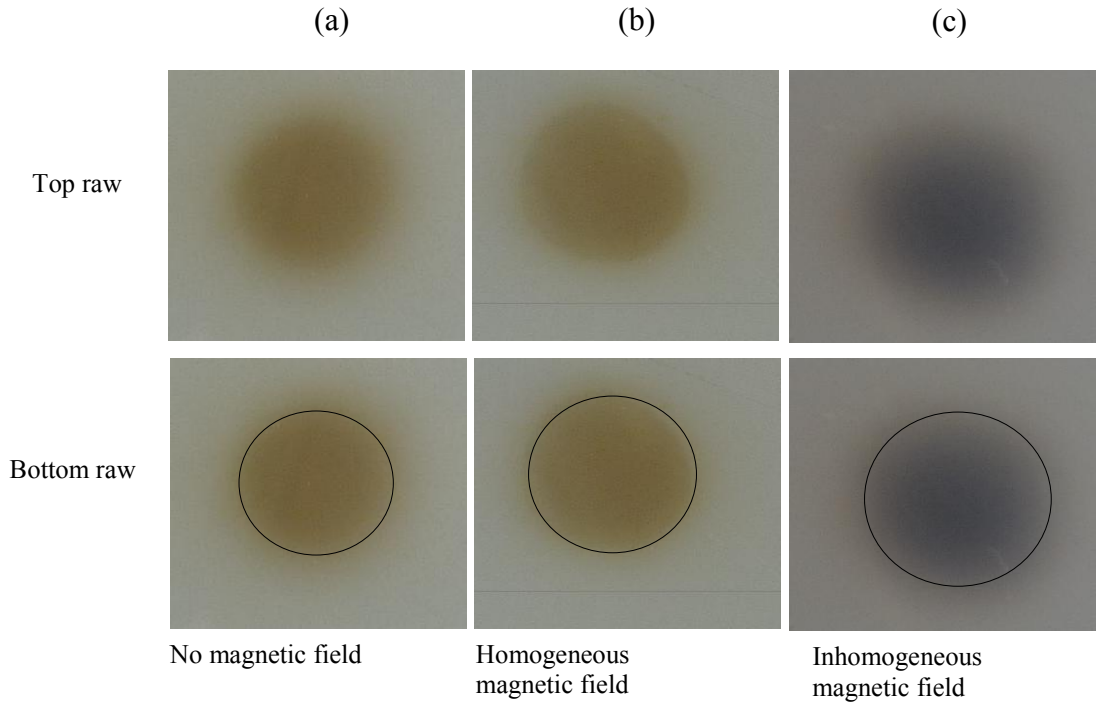

Figure 5.7: The spots of Ag- atoms at 30 mm away from the magnet

Figure 5.8 shows the deposits of silver observed on the glass slides of the target plate when the beam of Ag- atoms was collimated with a pair of slits. In this case the target plate was positioned 13 mm away from the magnet. The horizontal line on the left (a) is the reference, the deposit of silver that was observed when the atoms were not acted upon by any magnetic field. The horizontal line on the right (b) is the deposit of Ag- atoms that was observed when they were passed through the inhomogeneous magnetic field before they reached the target plate. It is longer and broader than the reference, as the Ag- atoms were pulled outward by the inhomogeneous magnetic field. The phenomenon illustrated by these two silver deposits was clearly observed after the coating with gold. Pictures of these deposits and their width after the glass slides were coated with gold are shown in figure 5.11.

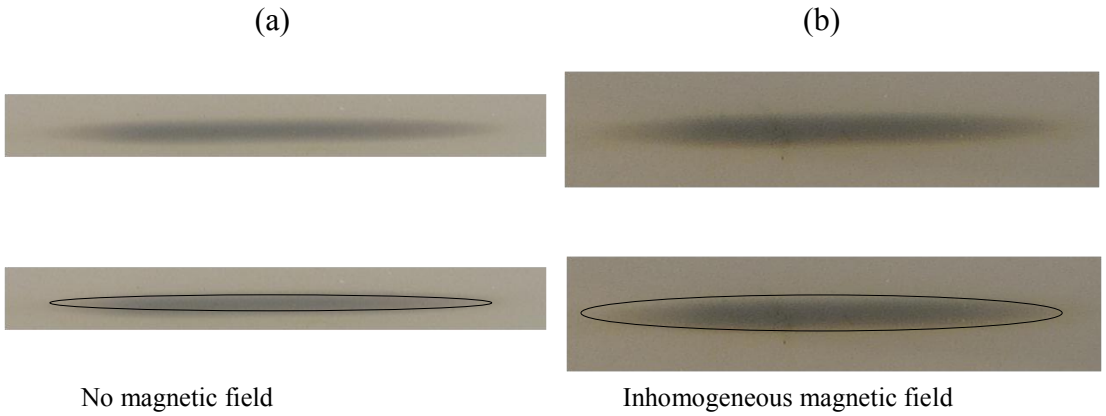

Figure 5.8: Deposits of Ag- atoms when the beam was collimated with a pair of slits

5.2.1.2 Results after the glass slides were coated with gold

Figure 5.9 shows the identical samples shown in figure 5.6 after the coating with gold. The arrangement of these spots is the same as in figure 5.6. Figure 5.9 (a) shows that the edge of the reference spot is not lighter than the centre of the spot after the glass slide has been coated with gold; instead, the spot has the same colour everywhere. Figures 5.9 (b) shows that the edge of the spot becomes lighter than the centre of the spot after the glass slide has been coated with gold. The lighter region of spot (c) is larger than the lighter region of spot (b).

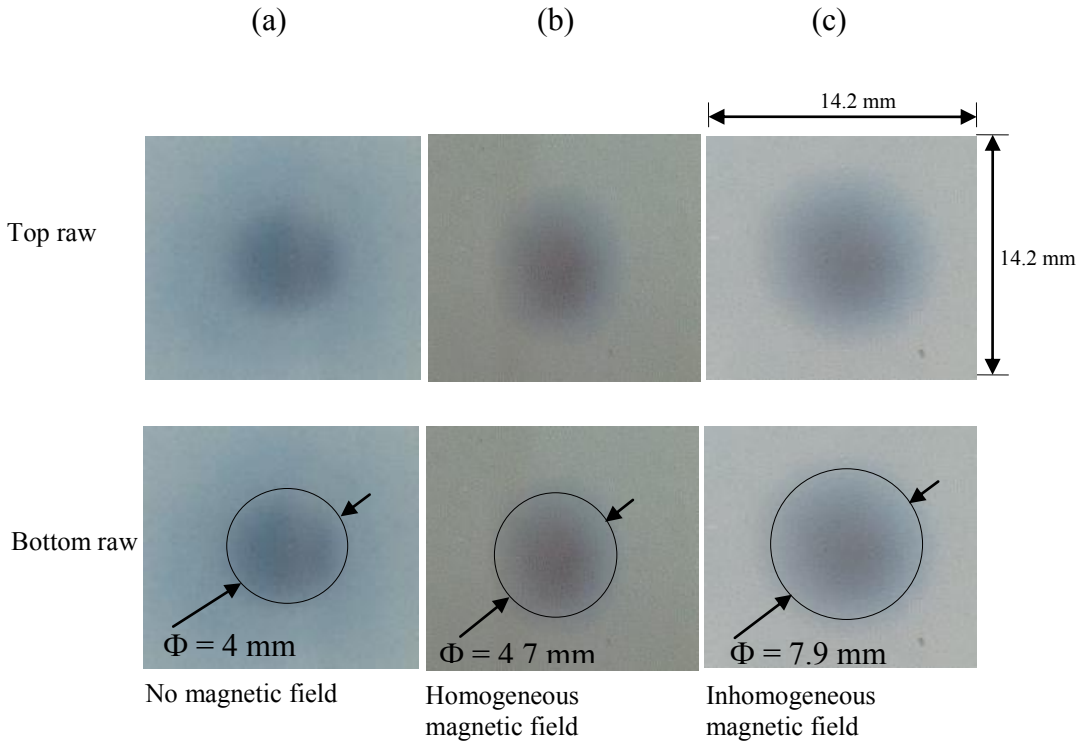

Figure 5.9: The spots of Ag- atoms at 13 mm away from the magnet after coating of the glass slides with gold

The diameters of the spots observed when the target plate was positioned at 13 mm are given in table 5.1. These diameters were used to calculate the deflection of Ag-atoms, which is also shown in the same table. Detailed calculations of deflection are shown in Appendix D. Table 5.1 shows that a maximum deflection of Ag- atoms caused by the homogeneous magnetic field with the target 13 mm from the magnet and the beam collimated by a pair of round- hole collimators is 0.32^{o}. This was not expected, as $F \propto \frac{\partial B}{\partial z}$. It also shows that the maximum deflection of Ag- atoms caused by the inhomogeneous magnetic field with the target 13 mm from the magnet and the beam collimated by a pair of round- hole collimators is 1.77^{o}. From a Maxwellian distribution, the average velocity of Ag- atoms at ~1 000 ^{o}C is $\bar{v}$ = 500 m/s, which resulted in a calculated deflection of 0.01^{o}, which is considerably lower than 1.77^{o}. This huge difference between the experimentally observed and calculated deflection raised a thought that maybe it is not only the Ag- atoms that were deflected but there was also a large fraction of Ag- ions (in the beam) that was deflected. The presence of Ag ions would be due to the following reasons: The tungsten wire that was coiled around the crucible was supplied with a current of ~ 6A, which resulted in thermal electrons being emitted and moving freely in a belljar. Thus, a fraction of Ag atoms coming out of the crucible was ionised by those electrons and became negative ions. The positive ions on the other had would be due to surface ionisation. This would be also the reason why the deflection was observed with a homogeneous magnetic field.

However, the calculation of a radius of curvature, r, of Ag- ions shown in Appendix D shows that r of each Ag- ion (both positive and negative) in a magnetic field used in this study would be only 1.61 mm. This means Ag- ions would curl when they reach a magnetic field and get stuck on magnetic circuit before they the target plate. Therefore there is no way they could be observed on a target plate. It was therefore clear that the size of the spot depends mostly on an expossure time given to a target plate. It is cannot be due a deflection of a beam as it was found to be theoretically impossible.

Table 5.1: Diameters of the spots of Ag- atoms at 13 mm away from magnet

Spot	(a)	(b)	(c)
Diameter	4 mm	4.7 mm	7.9 mm
Deflection	0	0.32^{o}	1.77^{o}

Figure 5.10 represents the same results as figure 5.7 after the glass slides were coated with gold. The arrangement of these spots is the same as in figure 5.7. Figure 5.10 (a) again shows that the edge of the reference spot is not lighter than the centre of the spot after the glass slide has been coated with gold; instead, the spot is homogeneous. Figures 5.10 (b) shows that the edge of the spot becomes lighter than the centre of the spot after the glass slide has been coated with gold, but the lighter region of spot (c) is larger than the lighter region of spot (b). The diameter of each of these spots is shown in table 5.2.

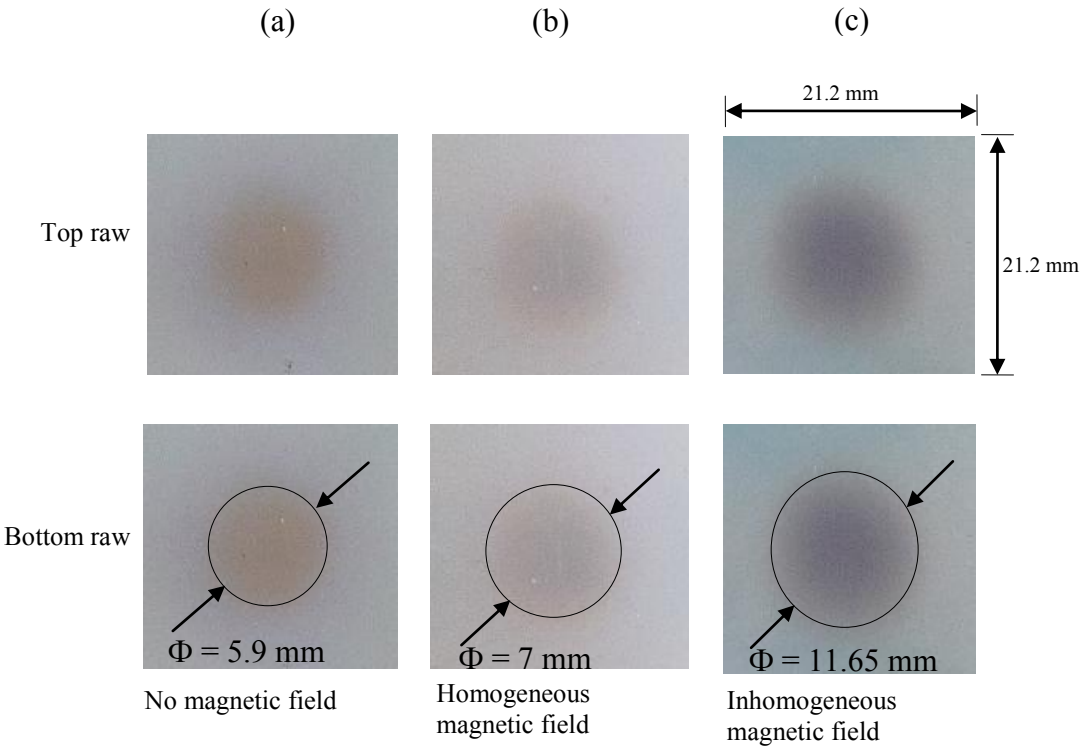

Figure 5.10: The spots of Ag- atoms at 30 mm away from the magnet after coating of the glass slides with gold

The diameters of the spots and deflection of Ag- atoms that were observed when the target plate was positioned at 30 mm and the beam collimated by a pair of round- hole collimators are given in table 5.2. The maximum deflection of Ag- atoms caused by a homogeneous magnetic field is 0.4^{o} (which was also not expected, as $F \propto \frac{\partial B}{\partial z}$). It also shows that the maximum deflection of Ag- atoms due to the inhomogeneous magnetic field is 2.05^{o}. In this case, a theoretically calculated deflection for $\bar{v} =$ 500 m/s is also 0.01^{o}, which is also significantly less than 2.05^{o}. This difference and the increase in the diameter of the spot observed when a beam was passed through a homogeneous magnetic field also indicate that the spot gets broader with the exposure time. The detail calculations of 0.4^{o} and 2.05^{o} are also given in Appendix D.

Table 5.2: Diameters of the spots of Ag- atoms at 30 mm away from magnet

Spot	(a)	(b)	(c)
Diameter	5.9 mm	7 mm	11.65 mm
Deflection	0	0.4^{o}	2.05^{o}

Figure 5.11 shows the identical samples shown in figure 5.8 after coating with gold. The reference deposit of Ag- atoms is shown in figure 5.11 (a). The coating of the glass slide with gold allowed the edge to be clearly seen. As a result, its width was measured to be 1.5 mm and its length was measured to be 16.5 mm. The deposit of Ag- atoms deflected in an inhomogeneous magnetic field is given in figure 5.11 (b). The coating of the glass slide with gold gave the deposit a roughly elliptical shape. If the beam consisted of atoms with the same speed, it would split completely into two separate beams in the presence of an inhomogeneous magnetic field. Owing to the different speeds experienced by the atoms, the deflection is not sharply pronounced. Figure 5.11 (c) shows the image of figure 5.11 (b) after it has been colour- only enhanced, which makes the elliptical deposit clearly visible. The deposit in figure 5.11 (c) was also colour- only enhanced in order to determine the dimensions of the elliptical deposit more accurately. The image of the deposit of silver was then clearly seen and is shown in figure 5.12 (a). The drawing with the dimensions of this image is given in figure 5.12 (b).

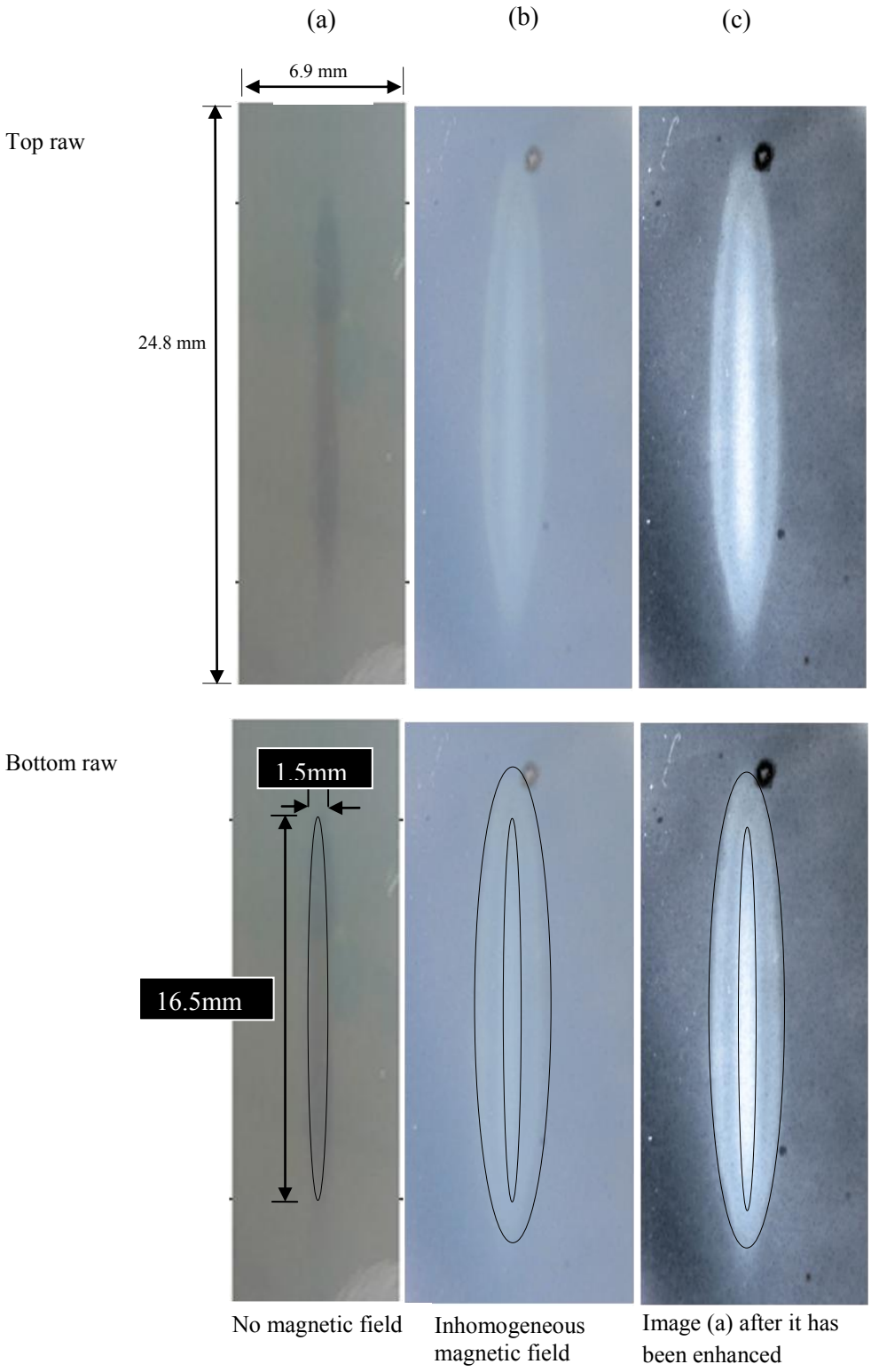

Figure 5.11: Deposits of Ag- atoms from the slit collimator with gold- coated glass slides after deposition

Figure 5.12 shows more detail of the elliptical deposit of Figure 5.11 (b). In figure 5.12 (a), the elliptical deposit is shown to consist of three regions. The core region is labelled G, the inner ring I and the outer ring O. The darkness of each region is an indication of the amount of silver deposited. It is seen that the inner ring has the most concentrated deposition of Ag- atoms. The core shows weak to no deposition of silver. This is attributed to the velocity distribution of the Ag- atoms following a Maxwellian distribution. The proportion of Ag- atoms with a velocity less than $\bar{v} =$ 500 m/s is greater than the proportion of Ag- atoms with a velocity greater than $\bar{v} =$ 500 m/s, and they were deposited on the inner ring I and the outer ring O, as they experienced a greater deflection. Hence, the inner ring I and outer ring O are darker than the core G.

In this case the deflection was measured using the dimensions of the elliptical deposit shown in Figure 5.12 (b) and dimensions of the reference deposit shown in Figure 5.11 (a). Table 5.3 shows the maximum deflection of Ag- atoms. Table 5.3 indicates a maximum deflection of 1.16^{o} in the positive and negative *z* directions (that is, towards B_{max} and towards B_{min}), giving the outer ring a width of 4.04 mm in figure 5.12. Table 5.3 shows that there is a maximum deflection of 1.12^{o} towards the positive and negative *x* directions, giving the outer ring a maximum width of 19 mm in figure 5.12. Again, the deflections 1.12^{o} and 1.16^{o} are greater than 0.01^{o}, which was theoretically calculated for the average velocity, and the first thing that would be thought of as a reason for such a huge difference between the theoretical and experimental results would be the presence of Ag- ions in the beam. Nevertheless, it has been already theoretically shown in Appendix D that there was impossible for Ag- ions to reach the target plate. Therefore this disagreement is also an indication that the size of each deposit on a glass slide depends mostly on its exposure time

Table 5.3: Deflection of Ag- atoms when the beam was collimated with a pair of slits

Maximum deflection to the positive and negative z direction	1.16^{o}
Maximum deflection to the positive and negative *x* direction	1.12^{o}

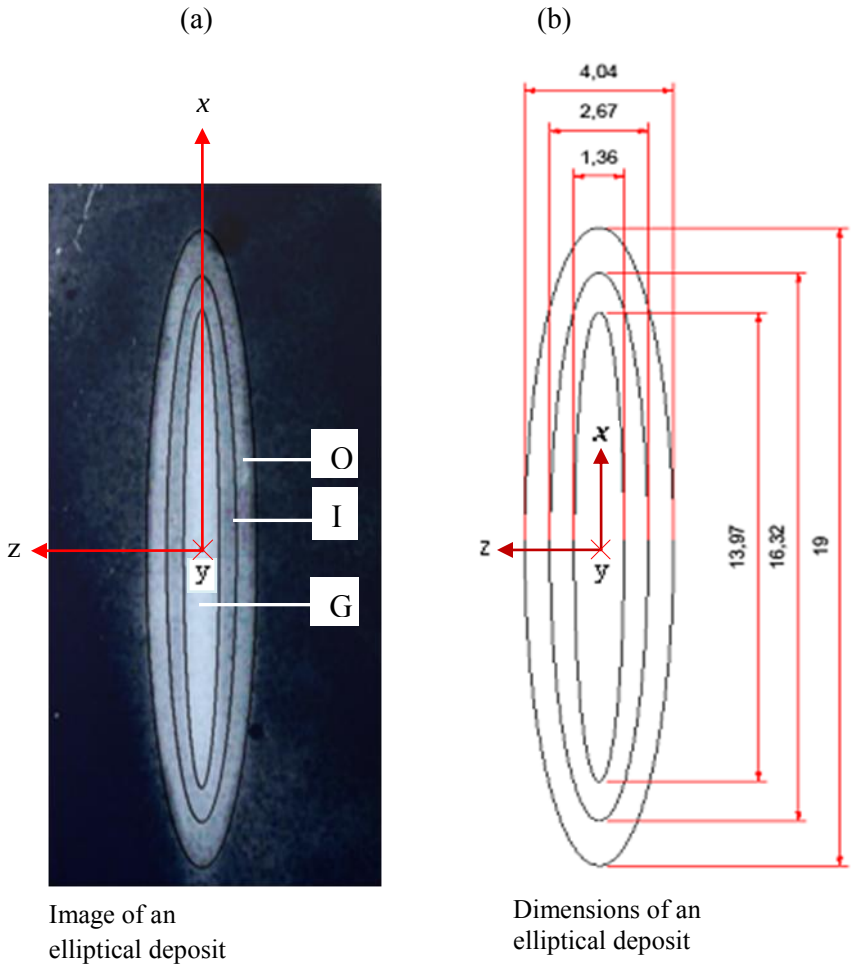

Figure 5.12: The image (a) and the dimension (b) of the silver deposit obtained

The maximum deflection obtained in table 5.3 is 0.65^{o} less than that was obtained when the round- hole collimators were used at the same distance from the target plate. This is because the width of the slit collimators is 0.5 mm less than the diameter of the round- hole collimators.

In addition to the analysis of the results, it should be mentioned that the deflection of Ag- atom beam could have been more accurately determined by doing RBS or PXIE measurements on the Ag deposits and for instance putting a Gaussian fit through the deposit. However, within a calculated 0.01^{o} deflection it was not worth it.

6 CHAPTER 6

DISCUSSION AND CONCLUSIONS

The main aim of this project was to design and construct the apparatus in which silver-109 atoms could be deflected with a homogeneous and inhomogeneous magnetic field and to make a recommendation on the suitability of the findings of this thesis project in relation to the idea of removing silver-110 atoms from helium by deflecting these atoms with an inhomogeneous magnetic field onto target plates situated on the inner perimeter of the helium pipe.

The possibility of deflecting Ag- atoms by an inhomogeneous magnetic field exists due to the fact that a Ag- atom consists of a nucleus and 47 electrons. The first 46 electrons form a "cloud'' with net angular momentum $J_1 = 0$. The 47th electron has a total angular momentum $j = l + s = 0 + s = 1/2\ \hbar$, as it is located in an s- orbital. As a result, the Ag- atom will have a total angular momentum equal to the total angular momentum of the 47th electron $j = s = 1/2\ \hbar$. The magnetic moment of the Ag- atom will be equal to the magnetic moment of the 47th electron $\mu_z = 9.270154 \times 10^{-24}$ J/T, where z is a direction of the magnetic field. Each Ag- atom experiences a deflecting force $F_z = \pm\mu_z \frac{\partial B_z}{\partial z}$, where $\frac{\partial B_z}{\partial z}$ is the gradient of the magnetic field. The deflection z of Ag- atoms that are travelling at a velocity v can be theoretically calculated by $z = F_z l_m \left(l_{mg} + \frac{l_m}{2} \right) \Big/ m v^2$ where m is the mass of a Ag- atom, l_{mg} is the distance of the target plate from magnet, l_m is the length of magnet and F_z is the deflecting force, which was 3.23×10^{-22} N in this study.

It should be emphasized that the deflection of Ag-atoms was not really observed as it was expected from the theoretical calculations. It can be also seen from the experimental set- up (distance between collimators, size of the slit, magnetic field gradient) that it would be in any case extremely difficult to observe any deflection. The reason being this set- up is much less sensitive compare the set- up of Gerlach who already struggled to observe the deflection. For this reason it was concluded that an apparatus in which silver-109 atoms could be produced was successfully designed and constructed, but the deflection of atoms with a magnetic field was unsuccessful as expected from the theoretical calculation.

In a helium pipe of a PBMR, the helium pressure is ~ 60 bar, which means that there is a mean free path of 1.65×10^{-8} m. It follows that if helium of this pressure were to be injected in a belljar when experiments were performed, the Ag- atoms would undergo 10^{11} collisions per second with helium atoms. The calculations of the mean free path and number of collisions are provided in Appendix D. Nevertheless, this means that the helium atoms would transfer some of their momentum $p = 1.9 \times 10^{-23}$ kg m/s to Ag-atoms, which have the momentum of 9.8×10^{-23} kg m/s, 10^{11} times per second. The calculations of the linear momentum of helium atoms and Ag- atoms at 1 000 ^{o}C are also shown in Appendix D. This would result in Ag- atoms beam not being deflected

at all because the force of deflection $F_z = 3.23\text{x}10^{-22}$ N due to a magnetic field is very weak.

Regarding the conclusion as PBMR is concern, applying a magnetic field gradient of at least as strong as the one used in this study is over approximately 1 m is not really feasible. To get that gradient the permanent magnets should be placed within the pipe, but at the temperature of 1 000 ^{o}C permanent magnets lose their properties. It is therefore the conclusion of this study that the technique of removing Ag- atoms from the hot coolant by deflecting them with an inhomogeneous magnetic field onto target plates situated on the inner perimeter of the hot outlet pipe will not be effective. As a result, it is recommended that further research be done to find another means of removing Ag- atoms from helium fluid.

7 BIBLIOGRAPHY

[Be09] Bentor, Y, Chemical Element.com, http://www.chemicalelements.com/elements/ag.html, [12 May, 2009]

[Be08] Bethlem, H. L., *Getting a Handle on Difficult Atoms*, *Physics 1*, Vol. 25, pp. 1-3, 2008

[Ch06] Charollais, F., CEA and AREVA R&D on HTR Fuel Fabrication and Presentation of the CAPRI Experimental Manufacturing Line, *Nuclear Engineering and Design*, Vol. 236, pp. 534–542, 2006

[De85] Dehmelt, H., Continuous Stern-Gerlach Effect: Principle of Idealized Apparatus, *Proceedings of the National Academy of Science*, Vol. 83, pp. 2291-2294, 1985

[Ei85] Eisberg, R. and Resnick, R., *Quantum Physics of Atoms, Molecules, Solids, Nuclei, and Particles*, John Wiley, New York, 1985

[Fl99] Fleisch, D. and Kraus, J.D., *Electromagnetics with Applications*, McGraw-Hill, New York, 1999

[Fu95] Fukuda, K. et al., Irradiation Behavior of HTGR Coated Particle Fuel at Abnormally High Temperature, *Nuclear Energy and Design*, Vol. 157, pp. 221-230, 1995

[Fu58] Funk, E. G. and Wiedenbeck, M. L., Decay of ^{110}Ag, *Physical Review*, Vol. 112, No. 4, pp. 1247-1251, 1958

[Fr09] Franklin, A., *Experiments in Physics*, Appendix 5: Right Experiment, Wrong Theory: The Stern-Gerlach Experiment, Stanford University, Germany, 2009

[Fri03] Friedrich, B. and Herschbach, D., *How a Bad Cigar Helped a Reorient Atomic Physics*, American Institute of Physics, USA, 2003

[Gr05] Greneche, D. et al., The AREVA HTR Fuel Cycle: An Analysis of Technical Issues and Potential Industrial Solutions, *Nuclear Energy and Design*, Vol. 236, pp. 635-642, 2005

[Hi97] Hinwood, B. G., *Science for the Health Professions*, Nelson Thornes, UK, 1997

[Ho78] Hobbie, R. K., *Intermediate Physics for Medicine and Biology*, John Wiley, New York, 1978

[Jo07] Joseph, L. et al., Standardization of ^{110}Ag at BARC, *Journal of Metrology Society of India*, Vol. 22, No. 4, pp. 225-229, 2007

[Ko09] Kotz, J. C. et al., *Chemistry and Chemical Reactivity*, Thomson Brooks, USA, 2009

[Ku88] Kuriacose, J. C. and Rajaram, J., *Chemistry in Engineering and Technology*, India Institute of Technology, India, 1988

[Kr88] Krane, K. S., *Introductory Nuclear Physics,* John Wiley, New York, 1988

[La03] L'Annunziata, M. F., *Radioactivity Analysis*, Academic Press, USA, 2003

[Li06] Liang, T. X. et al., Irradiation Performance and Modeling of HTR-10 Coated Fuel Particles, *Nuclear Energy and Design*, Vol. 236, pp. 1922-1927, 2006

[Li99] Lide, D. R., *Handbook of Chemistry and Physics*, 79th Edition, CRC press, USA, 1999

[Ll84] Lliffe, C. E., *Introduction to Nuclear Reactor Theory*, Manchester University Press, UK, 1984

[Lo79] Lovell, S., *An Introduction to Radiation Dosimetry*, Cambridge University Press, UK, 1979

[Ma09] MagNet, http://www.infolytica.com/downloads/trialeditions/MagNetTE.exe, [May 18, 2009]

[Ma09] Makgantshang, J., *Evaluation of the Efficiency of Inhomogeneous Magnetic Field in Deflecting Silver Atoms in the PBMR-Magnetic Isotope Scrubber (MIS), MASRT-Mini-Dissertation*, North University, South Africa, 2009

[Ma01] Massachusetts Institute of Technology, Quantization of Angular Momentum, http://web.mit.edu/8.13/www/jlexperiment/jlexp-18pdf, [22 February, 2001]

[Mo08] Moormann, R., Fission Product Transport and Source Terms in HTRs: Experience from AVR Pebble Bed Reactor, *Science and Technology Nuclear Installation*, Vol. 2008, pp. 1-14, 2008

[Mo02] Moragues, J. A. et al., Decay of ^{110}Ag to ^{110}Cd, *Nuclear Energy and Design*, Vol. 99, pp. 652-668, 2002

[Mu01] Murray, R. L., *Nuclear Energy: An Introduction to the Concepts, Systems, and Applications of Nuclear Processes*, Elsevier, North Carolina, 2001

[Og1985] Ogawa, T. et al., Release of Metal Fission Products from UO_2 Kernel of Coated Particle, *Journal of Nuclear Materials*, Vol. 135, pp. 18-31, 1985

[Pa01] Park, S. E. et al., Collimation of a Beam of Cesium Atoms by Optical Molasses, with Resulting in Longitudinal Beam Velocity, *Optics Communications*, Vol. 192, pp. 57-63, 2001

[Po03] Ponomarev-Stepnoi, N. N. et al., Development of Fast Helium Reactors in Russia, *Nuclear Energy and Design*, Vol. 94, pp. 1-8, 2003

[Sa01] Sawa, K. et al., Prediction of Fuel Performance and Fission Gas Release Behavior During Normal Operation of the High Temperature Engineering Test Reactor by JAERI and FZJ Modeling Approach, *Journal of Nuclear Science and Technology*, Vol. 38, No. 6, pp. 411-419, 2001

[Sa68] Sax, N. I., *Dangerous Properties of Industrial Materials*, Litton Educational Publishing, New York, 1968

[Sh02] Shapiro, J., *Radiation Protection*, La Editorial, USA, 2002

[Sc05] Schaffer, M. B., Powering the World with Nuclear Energy–Past, Present, and Inevitable Future, *Foresight*, Vol. 7, No. 2, pp. 41-53, 2005

[Sh02] Shultis, J. K. and Faw, R. E., *Fundamentals of Nuclear Science and Engineering*, CRC Press, USA, 2002

[Sl04] Slabber, J., Pebble Fuel Advantages, *2nd International Topical Meeting on High Temperature Reactor Technology*, Beijing, China, September 22-24, 2004

[Sl55] Slater, J. C., *Modern Physics*, McGraw-Hill, New York, 1955

[Su84] Sullivan, M. F. et al., Effect of Oxidizing and Reducing Agent on Absorption of Neptunium from the Gastrointestinal Tract of Mice and Adult or Neonatal Rats, *Radiation Research*, Vol. 100, pp. 519-526, 1984

[Sy97] Syed, A. N., *Electric Machines and Electromechanics*, 2nd Edition, Schaums's outlines, McGraw-Hill, New York, 1997

[Me04] van der Merwe, J. J., Development and Validation of Fission Product Release Model and Software at PBMR, *2nd International Topical Meeting on High Temperature Reactor Technology*, Beijing, China, September 22-24, 2004

[Me08] van der Merwe, J. J. and Clifford, I., Development and Application of the PBMR Fission Product Release Calculation Model, *Nuclear Engineering and Design*, Vol. 238, pp. 3092-3101, 2008

[Ve01] Verfondern, K. et al., Modeling of Fuel Performance and Metallic Fission Product Release Behavior During HTTR Normal Operating Conditions, *Nuclear Engineering and Design*, Vol. 210, pp. 225–238, 2001

[We01] Weil, J., Pebble-Bed Design Returns [nuclear reactor], *Institute of Electrical and Electronics Engineering*, Vol. 38, pp. 37-40, 2001

[Zh08] Zhu, S. et al., Coupling of Modular High-Temperature Gas-Cooled Reactor with Supercritical Rankine Cycle, *Science and Technology of Installation*, Vol. 2008, pp. 1-9, 2008

APPENDIX A: MANUFACTURING DRAWINGS

The purpose of this appendix is to show the engineering drawings of the components of a designed and constructed apparatus.

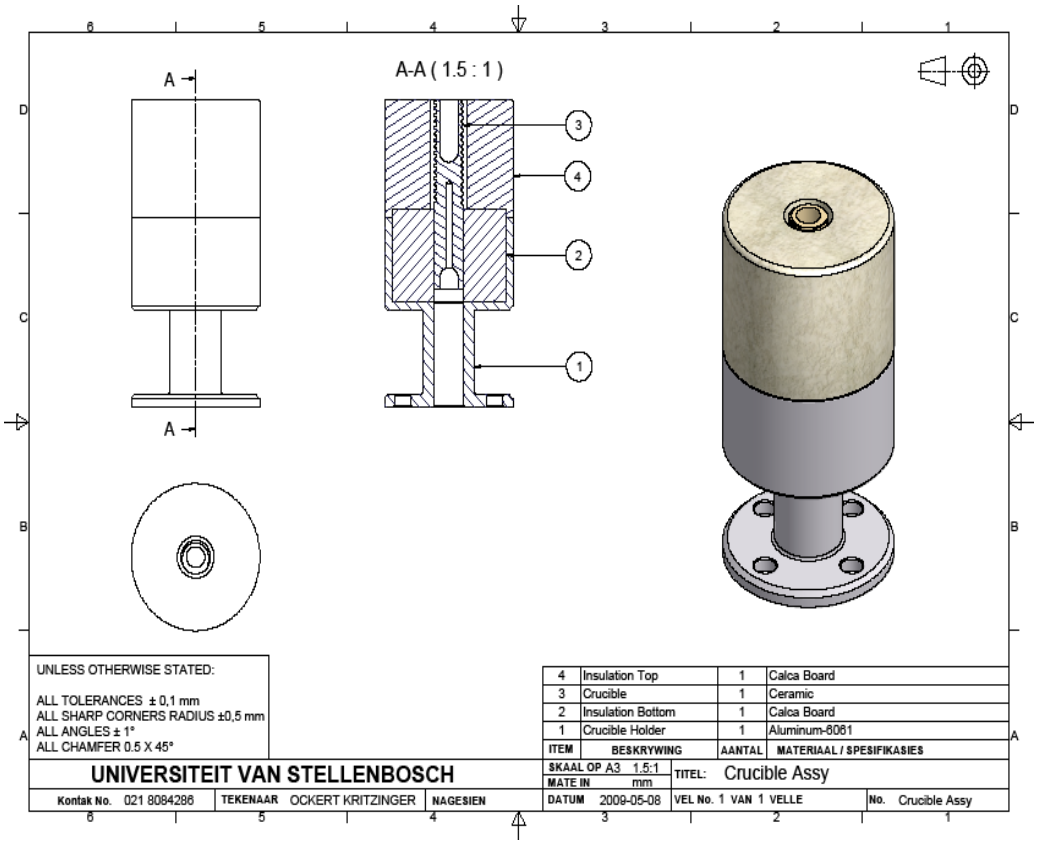

Figure: A1 Thermally insulated crucible

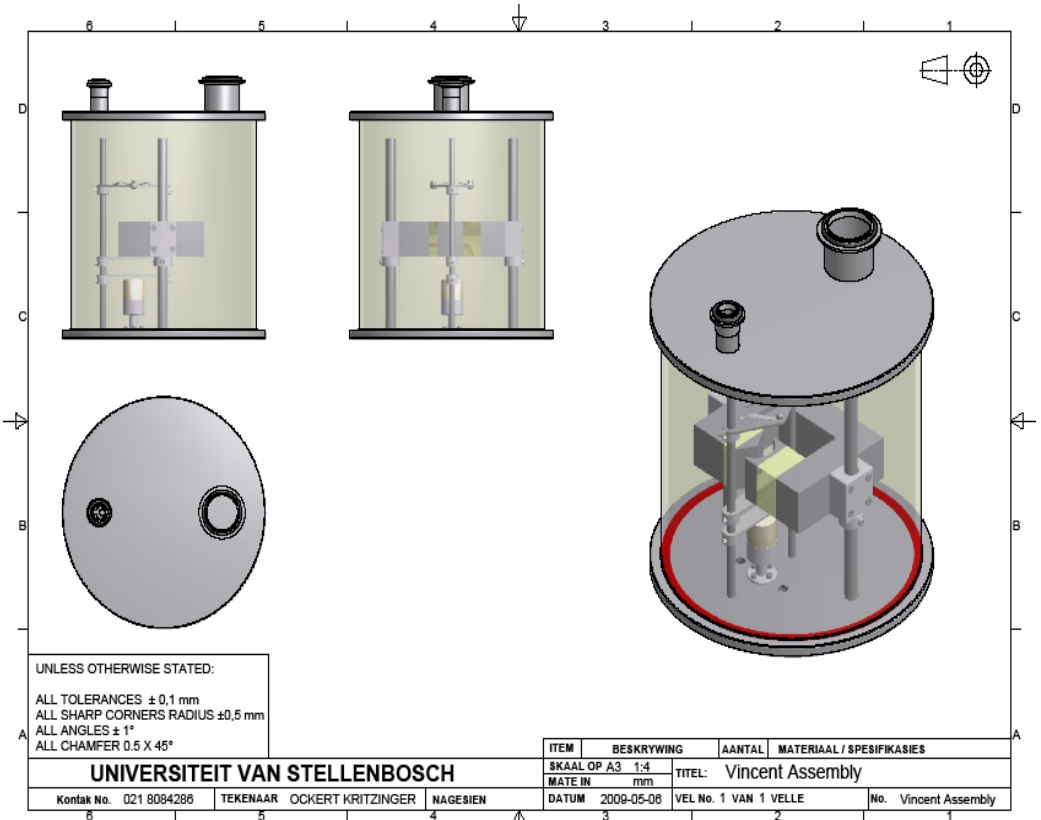

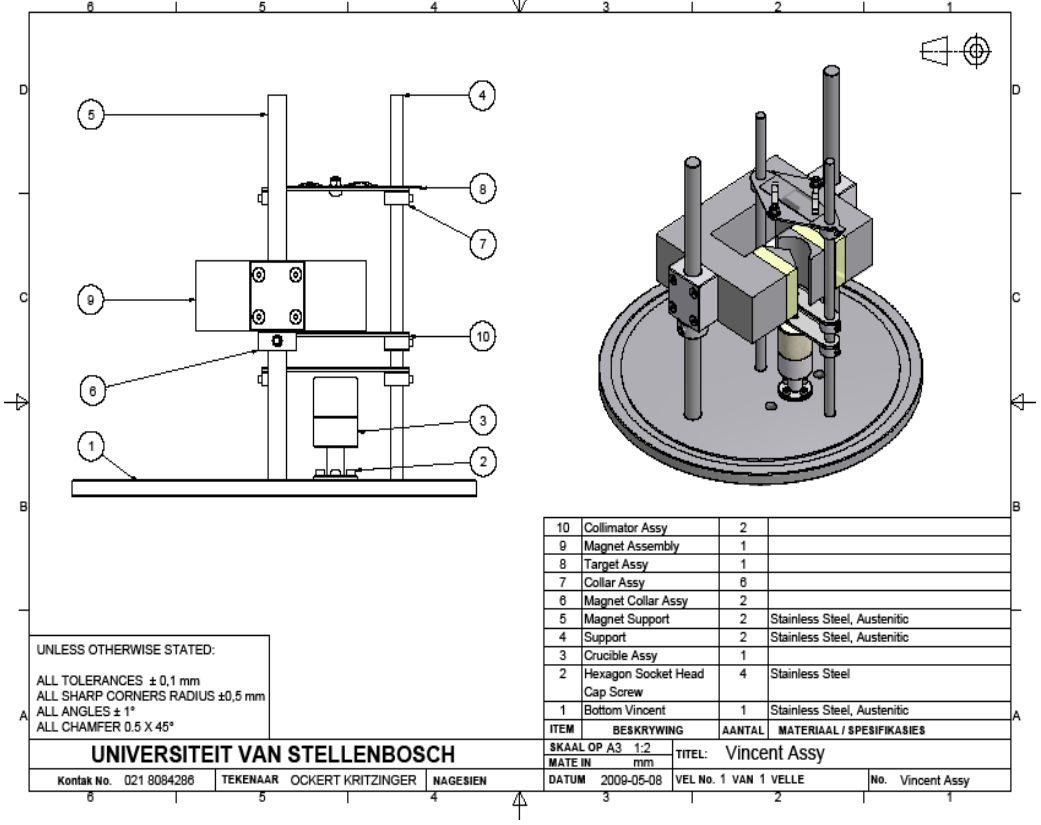

Figure A2: Experimental set-up

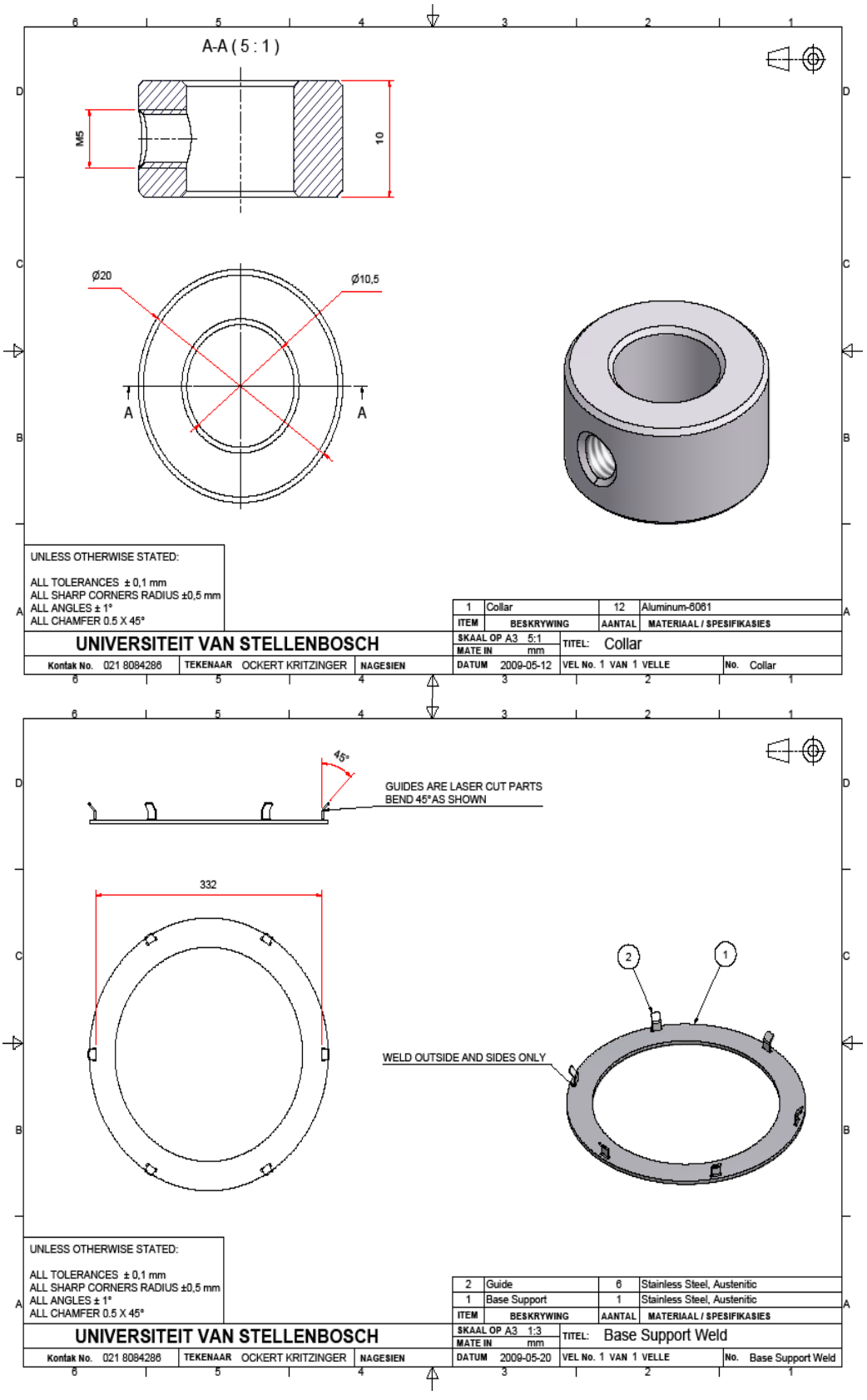

Figure A3: The collar that allowed the adjustment of the height of a target plate and the support for the belljar

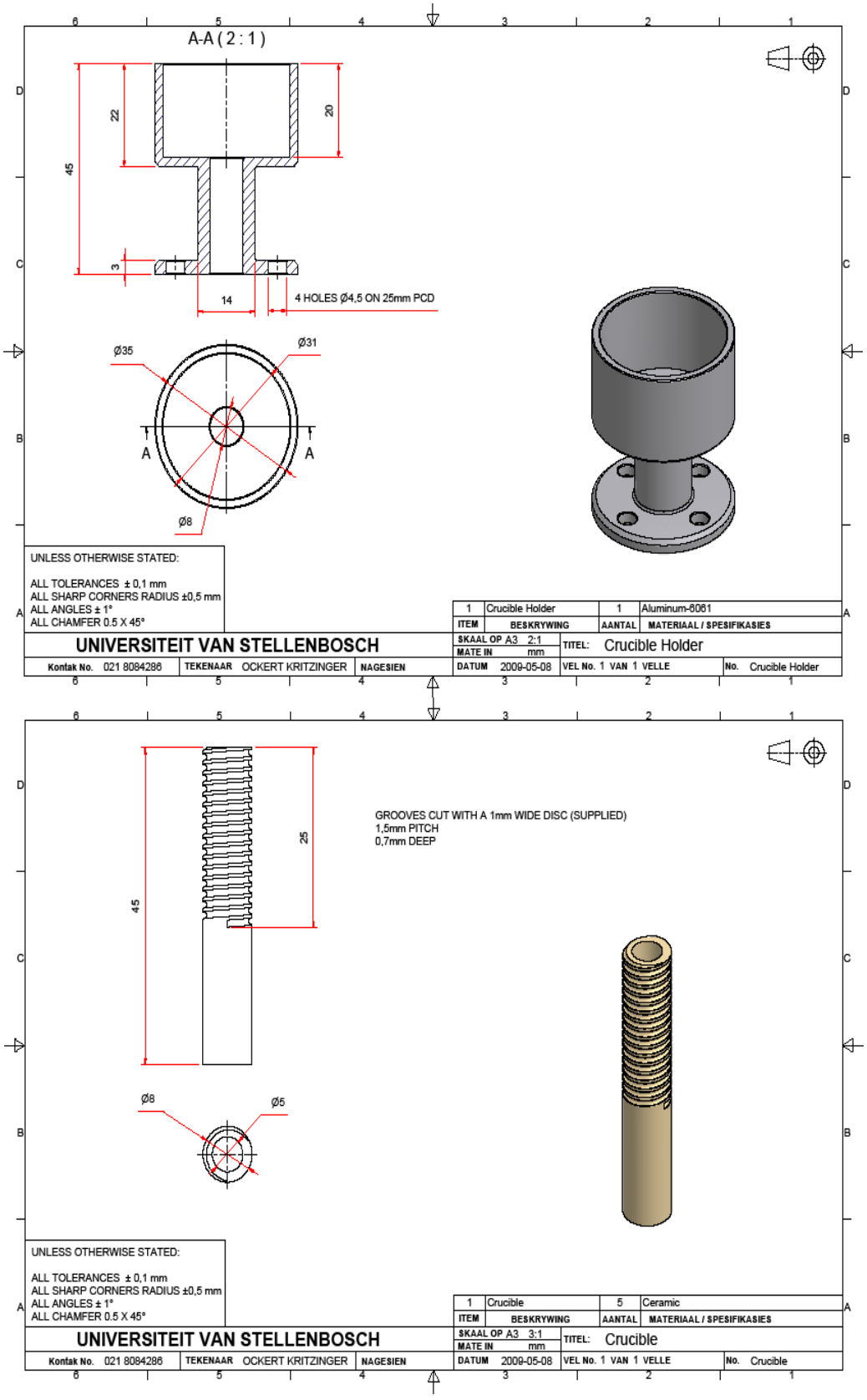

Figure A4: Crucible holder and the crucible

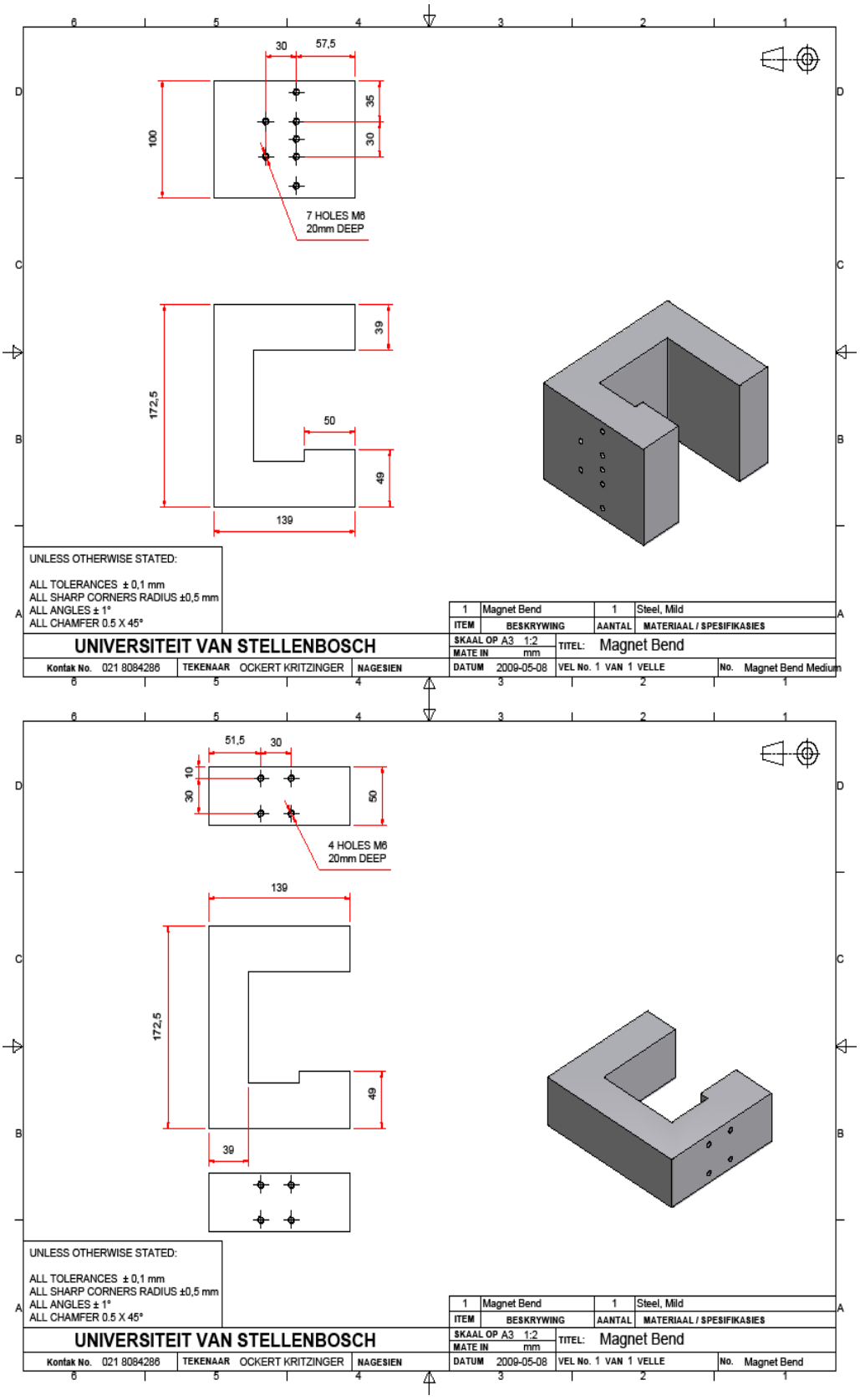

Figure A5: Magnet bend on which the wedge that makes an inhomogeneous magnetic field was mounted

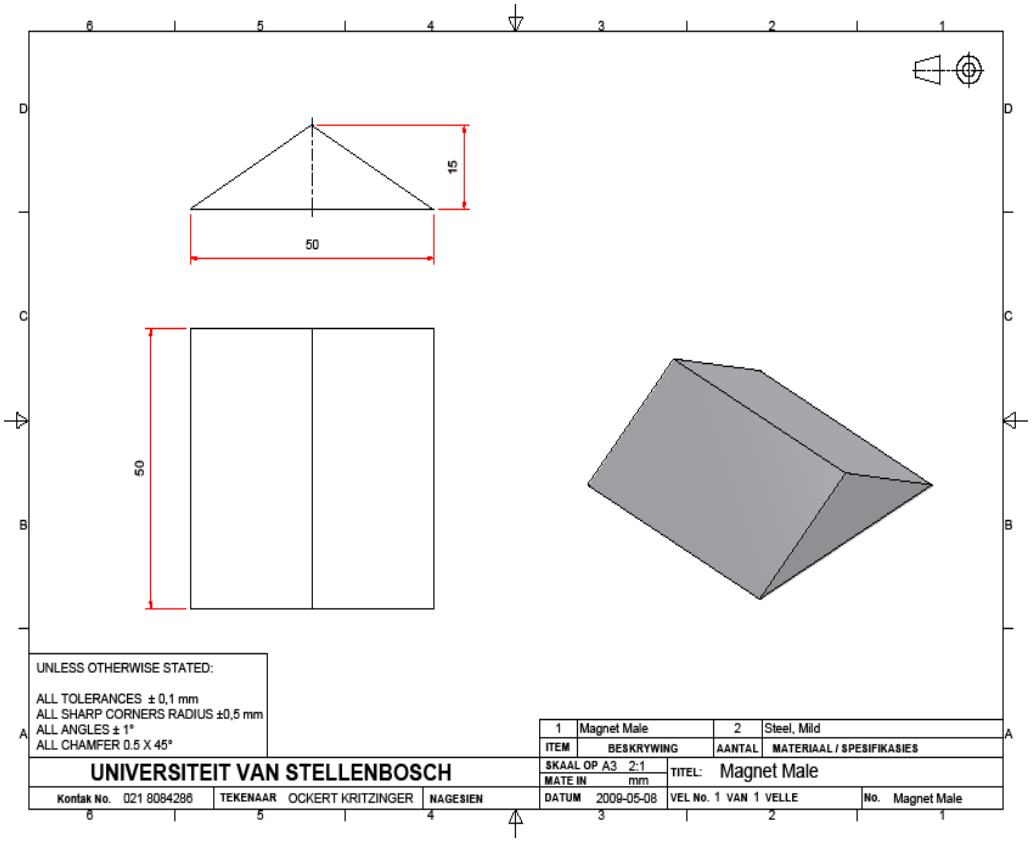

Figure A6: The wedge that makes an inhomogeneous magnetic field in a gap of a magnetic circuit

APPENDIX B: EXAMINED MAGNETIC FIELD GEOMETRIES

The purpose of this appendix is to show different geometries of the magnetic circuit of which performance in terms of the strength and inhomogeneity of the magnetic field in a gap was examined. This was done by using MagNet software, Trial Edition 2.26.2. For each figure, each part that represents a magnet is labeled and the rest is iron. The lines that appear are magnetic field lines. The minimum and maximum values of B in the gap, and the length of the gap l_g (l_g is from the point where B_{min} occurs to the point where B_{max} occurs) are shown at the bottom of the picture. The geometry in figure B1 is the one that was used in this study, for the reason that this geometry seemed to produce the most inhomogeneous magnetic field in the gap.

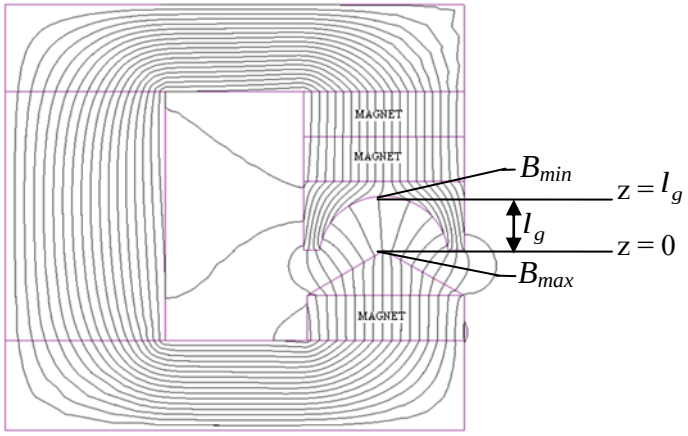

Figure B1: A magnetic circuit with l_g = 18 mm, B_{max} = 1.04 T and B_{min} = 0.24 T

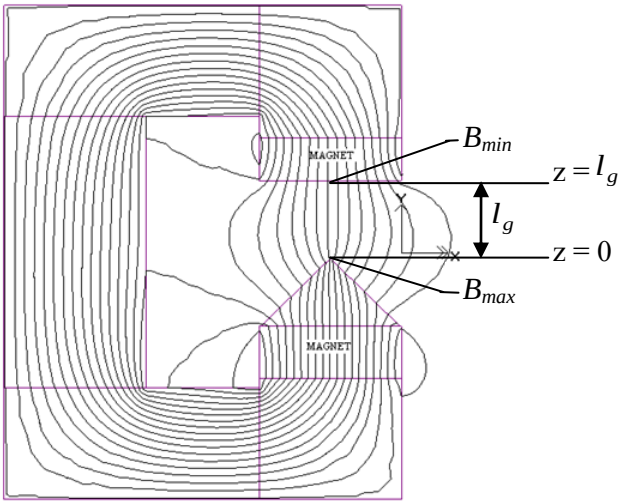

Figure B2: A magnetic circuit with l_g = 28 mm, B_{max} = 1.02 T and B_{min} = 0.51 T

In figure B1, the three magnetic field lines in the centre of the gap show that the magnetic field is inhomogeneous where the Ag- atom beam is to pass through. The magnetic field in the gap is fairly strong, as it ranges between 0.24 and 1.04 T. In figure B2, the magnetic field is strong compare to the one in figure B1, because it ranges between 0.51 and 1.02 T, while in figure B1, it ranges between 0.24 and 1.04 T. However, the field lines in figure B2 are not as inhomogeneous as in figure B1. In figures B3, B4, B5, B6, B7, B8, and B9 below, the magnetic field lines in the gap show that the magnetic field in the gap is not as inhomogeneous as in figure B1. In addition, the minimum and maximum values of the magnetic field (the values of B_{max} and B_{min}) in the gap show that the magnetic field is not as strong as in figure B1.

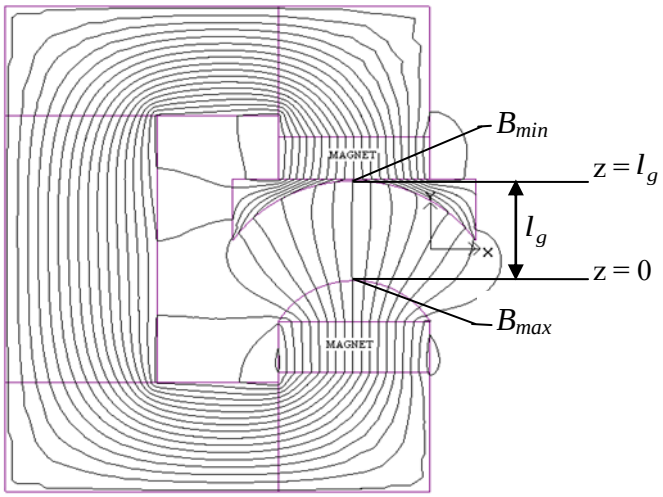

Figure B3: A magnetic circuit with l_g = 28 mm, B_{max} = 0.46 T and B_{min} = 0.32 T

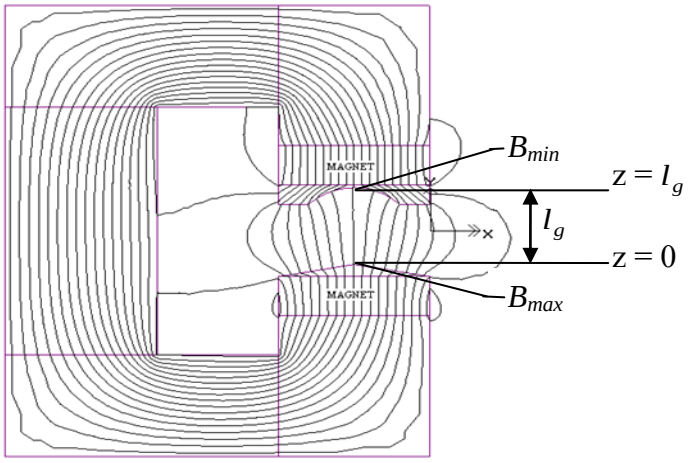

Figure B4: A magnetic circuit with l_g = 28 mm, B_{max} = 0.52 T and B_{min} = 0.28 T

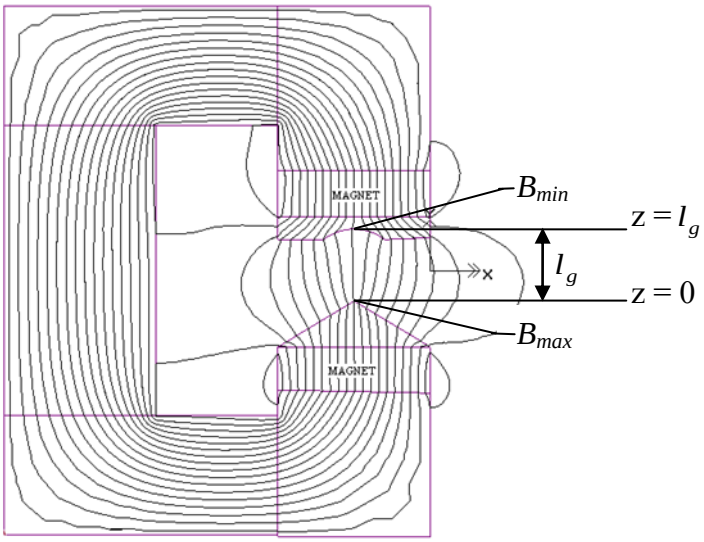

Figure B5: A magnetic circuit with l_g = 28 mm, B_{max} = 0.798 T and B_{min} = 0.313 T

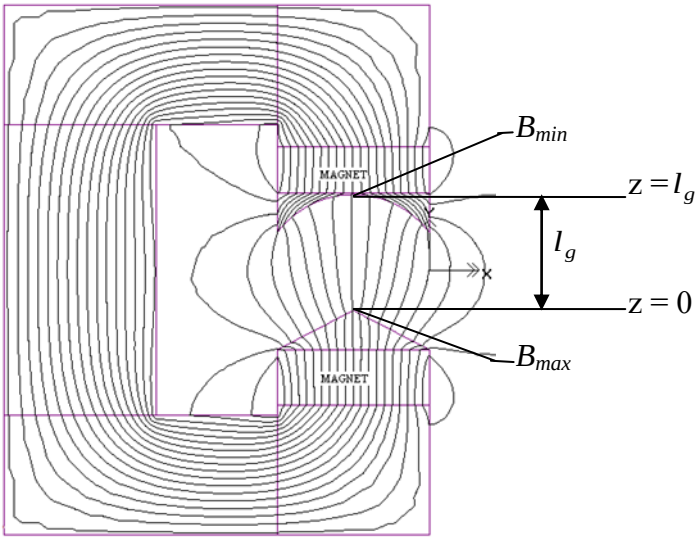

Figure B6: A magnetic circuit with l_g = 28 mm, B_{max} = 0.688 T and B_{min} = 0.293 T

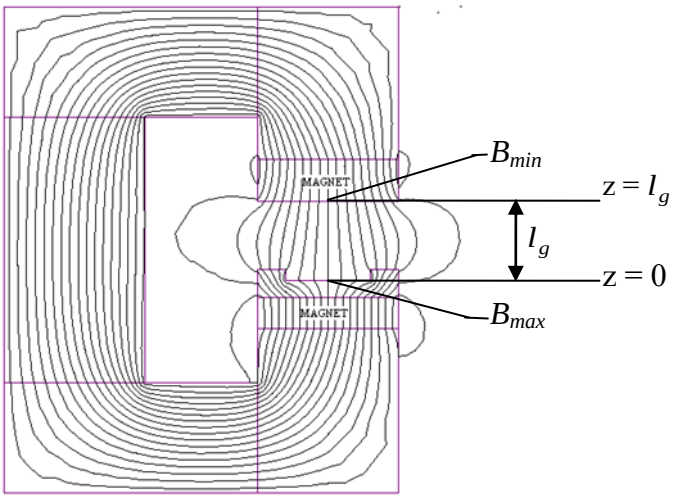

Figure B7: A magnetic circuit with l_g = 28 mm, B_{max} = 0.549 T and B_{min} = 0.375 T

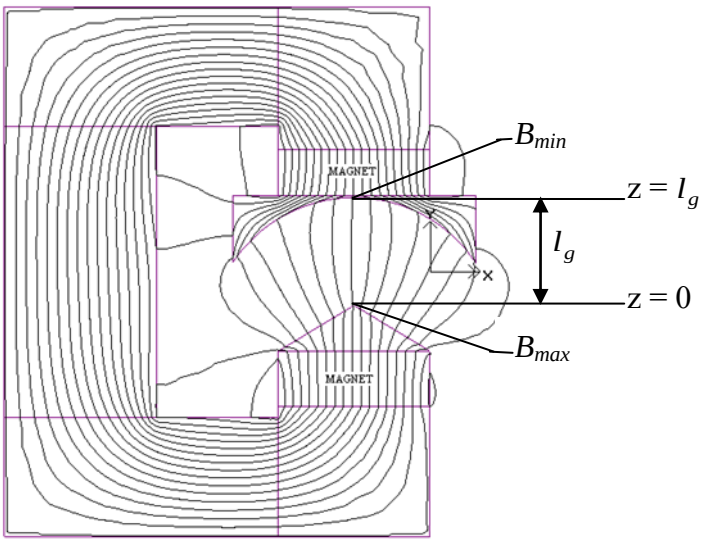

Figure B8: A magnetic circuit with l_g = 28 mm, B_{max} = 0.740 T and B_{min} = 0.319 T

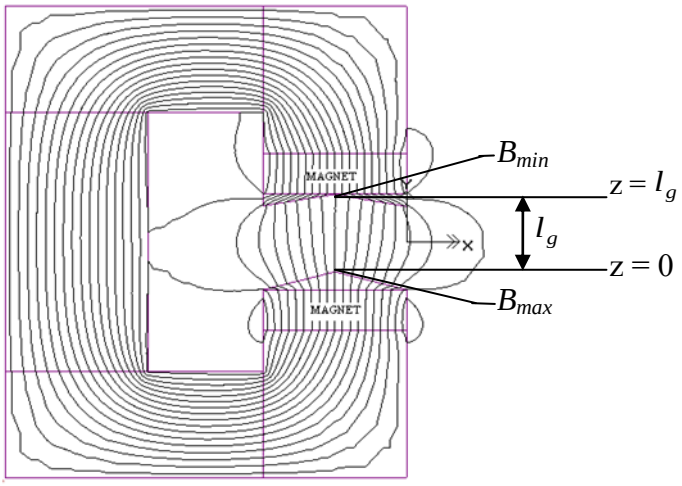

Figure B9: A magnetic circuit with l_g = 28 mm, B_{max} = 0.705 T and B_{min} = 0.31 T

APPENDIX C: VISUAL BASIC CODE

The purpose of this appendix is show the Visual Basic code that was used to calculate the magnetic field gradient at a position of the beam in the gap of the magnetic circuit and the deflection of atoms in the beam. The algorithm and the flowchart of the code are also included.

```
'This code computes the magnetic field gradient in the gap of the magnetic circuit and
the deflection of Ag-atoms
Private Sub CommandButton1_Click()

'Declaration of variables
Dim Z_deflection, z, z_plus_h, lm, m, v, F, h, D, lmg, B_of_z_plus_h,
B_of_z_minus_h, Gradient_of_B_at_z,
Gradient_of_B_at_a_position_of_the_beam_in_the_air_gap, counter1, counter2 As
Single

'Reading the values of lmg, lm and m from the spread sheet
lmg = Worksheets("sheet1").Cells(4, 14).Value
lm = Worksheets("sheet1").Cells(4, 13).Value
 m = Worksheets("sheet1").Cells(2, 12).Value

' Starting a for loop
For counter1 = 1 To 999
   'Reading the values of B_of_z_minus_h and B_of_z_plus_h from a spread sheet
   B_of_z_minus_h = Worksheets("sheet1").Cells(counter1+1, 3).Value
   B_of_z_plus_h = Worksheets("sheet1").Cells(counter1 + 3, 3).Value

   'Computing a Gradient of the magnetic field (B) at each at each point z
   Gradient_of_B_at_z = (B_of_z_plus_h - B_of_z_minus_h) / (2 * 0.0018)

   'Displaying a value of the gradient
   Worksheets("sheet1").Cells(counter1 + 2, 4).Value = Gradient_of_B_at_z

'Reading the value of the magnetic field gradient at the position of the beam
 Gradient_of_B_at_a_position_of_the_beam_in_the_air_gap =
Worksheets("sheet1").Cells(361, 4).Value

'Computing the magnitude of the deflecting force in Newtons
F = (9.270154 * 10 ^ (-24)) * (-
Gradient_of_B_at_a_position_of_the_beam_in_the_air_gap) *     100

 'Displaying the magnitude of the deflecting force
Worksheets("sheet1").Cells(4, 11).Value = F

'Ending a for loop
Next counter1
```

```
'Starting another for loop
For counter2 = 1 To 24

    'Reading the value of the speed in each cell
    v = Worksheets("sheet1").Cells(counter2 + 6, 14).Value

    'Computing the deflection in mm
    Z_deflection = 1000 * (F * (lm * (lmg + 0.5 * lm))) / (m * (v ^ 2))

    'Displaying the deflecting force
    Worksheets("sheet1").Cells(counter2 + 6, 15).Value = Z_deflection
'Ending a for loop
Next counter2
End Sub
```

An algorithm of the above code is the following:

Start
Declare variables
Creating a loop which reads a magnitude of the magnetic field at each point in the gap of the magnetic circuit
Compute a gradient of the magnetic field at each point in the gap of the magnetic circuit, and output it in the spreadsheet
Read a value of the gradient of the magnetic field at the position of the beam in the gap of the magnetic circuit
Compute the force of deflection
Display it in the spread sheet
End loop

Create the loop which reads the value of the speed of atoms from each cell in the spreadsheet
Compute a deflection as a function of speed and display it in the spreadsheet
End loop
End

The flowchart of the above code is the following:

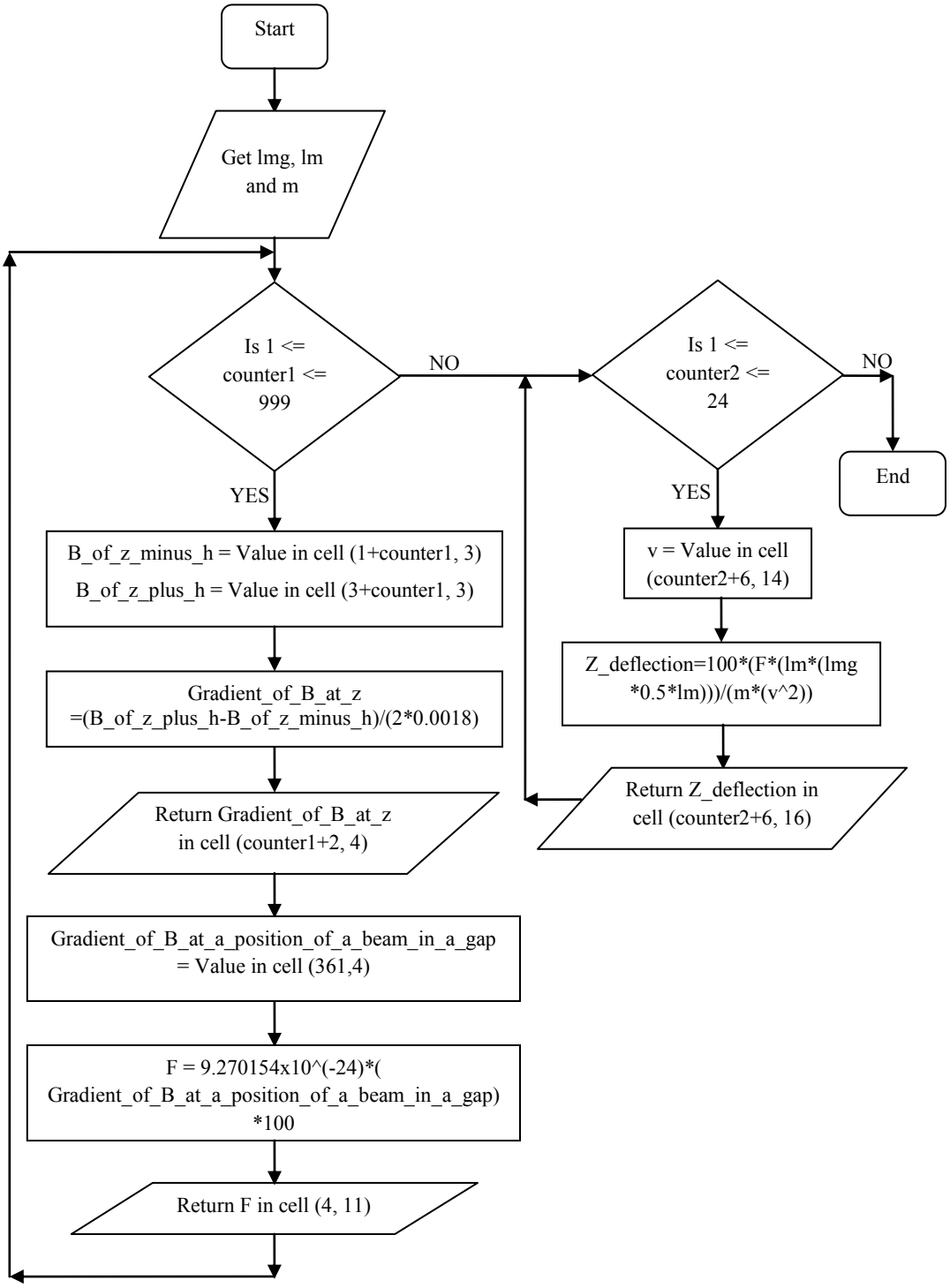

APPENDIX D: DETAIL CALCULATIONS

The purpose of this appendix is to show detail calculations of deflection of atoms from dimensions of the experimentally observed deposits of Ag-atoms, theoretical calculation of deflection for the average velocity of Ag-atoms at 1 000 ^{o}C, calculation of the mean free path in the helium pressure of 60 bar and the linear momenta of Ag-atoms and helium atoms at 1 000 ^{o}C.

Calculation of deflection of Ag-atoms using dimensions of the silver deposits that were observed on the glass slides

The calculations were based on Figure D1. For the case where the beam was collimated by a pair of round-hole collimators, t represents a radius of the spot observed on the glass slide. In the calculation for the case where atoms were collimated by a pair of slit collimators, t represents a length and a width of a reference deposit as well as the width of the elliptical deposit towards the positive (or negative) x direction and the width towards positive (or negative) z direction. A gap between the collimator and the magnetic circuit was not taken into account in these calculations. The reason being the magnetic circuit was sitting on the collimator when the experiments were performed.

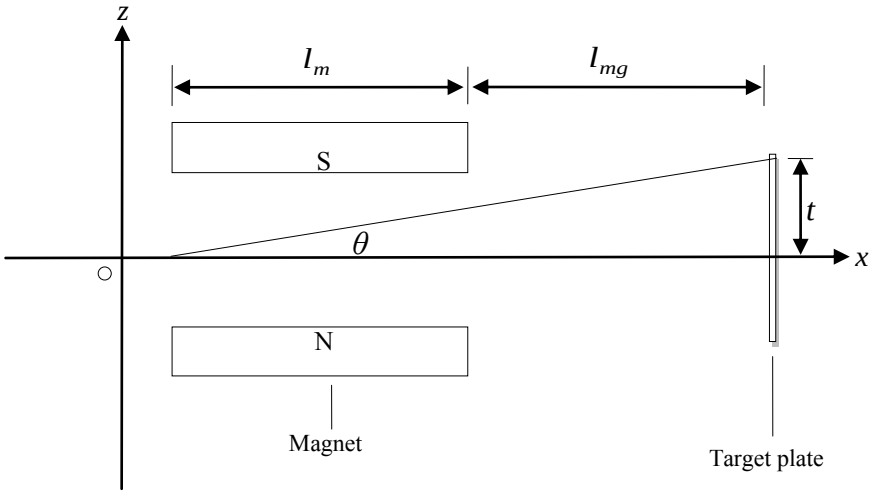

Figure D1 Approximation of deflection of Ag-atoms.

When a beam of Ag-atoms was collimated with a pair of round-hole collimators and a target plate positioned at 13 mm from the magnetic circuit, a diameter of a reference spot was found to be 4 mm which means that $t = 2$ mm.

Hence $\theta = \tan^{-1}\left(\frac{t}{l_m + l_{mg}}\right) = \tan^{-1}\left(\frac{2\text{mm}}{50\text{mm} + 13\text{mm}}\right) = 1.82^{o}$.

The diameters of the spots observed with a target plate positioned 13 mm from the magnetic circuit, the beam collimated by a pair of round-hole collimators and passed through a homogeneous and inhomogeneous magnetic field is 4.7 and 7.9 mm respectively. It means that $\theta = \tan^{-1}\left(\frac{t}{l_m + l_{mg}}\right) = \tan^{-1}\left(\frac{2.35\text{mm}}{50\text{mm}+13\text{mm}}\right) = 2.14^{\text{o}}$ for the spot of 4.7 mm diameter and $\theta = \tan^{-1}\left(\frac{t}{l_m + l_{mg}}\right) = \tan^{-1}\left(\frac{3.95\text{mm}}{50\text{mm}+13\text{mm}}\right) = 3.59^{\text{o}}$ for the spot of 7.9 mm diameter. It follows that a deflection of Ag-atoms by a homogeneous magnetic field is $2.14^{\text{o}} - 1.82^{\text{o}} = 0.32^{\text{o}}$ and a deflection due to inhomogeneous magnetic field is $3.59^{\text{o}} - 1.82^{\text{o}} = 1.77^{\text{o}}$.

Similarly, the deflection Ag-atoms collimated with a pair of round-hole collimators and observed with a target plate positioned 30 mm from the magnetic circuit is 0.4^{o} due to the homogeneous magnetic field and 2.05^{o} due to the inhomogeneous magnetic field. For the case where a beam was collimated by a pair of slit collimators and the target plate positioned 13 mm from the magnetic circuit, the deflection is 1.12^{o} towards the positive and negative x direction and 1.16^{o} towards the positive and negative z direction.

Theoretical calculation for deflection performed at $\bar{v} =$ 500 m/s, the average velocity of Ag-atoms at 1000°C

It can be seen from figure 4.10 that a measured flux density in a gap of a magnetic circuit can be expressed as $B = 2\text{x}10^{-5}x^4 - 0.001x^3 + 0.017x^2 - 0.154x + 0.9$ at any point x. A derivative of B with respect to x is $8\text{x}10^{-5}x^3 - 0.003x^2 + 0.034x - 0.154$, but $x = 7.2$ mm at a position of a beam. There a magnetic field gradient at a position of a beam is $8\text{x}10^{-5}(7.2)^3 - 0.003(7.2)^2 + 0.034(7.2) - 0.154 = -34.86$ T/m. Hence the force of deflection is $F_z = -3.23\text{x}10^{-22}$ N.

The mass of Ag-atoms is $1.808\text{x}10^{-22}$ g and the absolute value of the force $3.23\text{x}10^{-22}$ N was used to calculate deflection as the amount of deflection was more of the interest than its direction. Hence the deflection of Ag-atoms at $\bar{v} =$ 500 m/s, $l_m = 50$ mm and $l_{mg} = 13$ mm is given by

$$z = F_z l_m \left(\frac{l_{mg} + \frac{l_m}{2}}{mv^2}\right) = 161.5\text{x}10^{-22}\,\text{N}\cdot\text{mm}\left(\frac{13\text{mm} + \frac{50\text{mm}}{2}}{1.808\text{x}10^{-22}\,\text{g}\left(500\text{x}10^3\,\text{mm/s}\right)^2}\right)$$

$$= 1.36\text{x}10^{-2}\ \text{mm}$$

Now $1.36\text{x}10^{-5}$ m must be converted to an angle and this is done as followings:

$tan\theta = \frac{z}{l_{mg}+l_m} = \frac{1.36x10^{-2}\,mm}{63mm}$ which means that θ = 0.01°. Therefore a theoretical deflection of Ag-atoms at $\bar{v}$ = 500 m/s, l_m = 50 mm and l_{mg} = 13 mm is 0.01°

Similarly, a deflection of Ag-atoms at $\bar{v}$ = 500 m/s, l_{mg} = 30 mm and l_m = 50 mm is also approximately 0.01°.

Calculation of the mean free path for helium pressure of 60 bar at 1 000 °C

The pressure of helium in a PBMR coolant pipe is 60 bar. In this study the temperature in a belljar was ~ 1 000 °C. It follows that the injection of helium into the belljar would result in a mean free path of $\lambda = \frac{(1273K)(1.38X10^{-23}\,J/K)}{4\pi\sqrt{2}(10^{-10}\,mm)^2(60x10^5\,Pa)} = 1.65x10^{-8}$mm within the belljar. The root mean square velocity of Ag-atoms at 1 000 °C is 540 m/s. This means that $t_{mean} = \frac{1.65x10^{-8}\,m}{540m/s} = 3.06x10^{-11}$ s. Therefore each Ag- atom would undergo 10^{11} collisions with helium atoms per second.

Calculation of the linear momenta of helium atoms and Ag- atoms.

From a Mxwellian distribution of velocity the average speed is given by $\bar{v} = \sqrt{\frac{3kT}{m}}$ where k = 1.38x10^{-23} J/K. The molar mass of a helium atom is 6.68x10^{-27} kg. This means that the average velocity of helium atoms at 1 000 °C is $\bar{v} = \sqrt{\frac{3kT}{m`}} = \sqrt{\frac{3\times1.38\times10^{-23}\,J/K\times1273K}{6.68\times10^{-27}\,kg}}$ = 2808 m/s. Hence, on average the linear momentum of a helium atom at 1 000 °C is $p = m\bar{v} = 6.68\times10^{-27}\,kg\times2808m/s$

= 1.9 x10^{-23} kg m/s

Similarly the linear momentum of Ag-atoms at 1 000 °C is 9.8x10^{-23} kg m/s

Calculation of the radius of curvature of a Ag- ion in a gap of a magnetic circuit

A radius of curvature of a charged particle due a magnetic field is given by $r = \frac{mv}{qB}$ where m is a mass, v is a velocity, q is a charge and *B* is a magnetic field. Assuming a 1-charge state of a positive Ag-ion, using v = 500 m/s, *B* = 0.35 T (the

magnetic field at the position of a beam in a gap of a magnetic circuit, x =7.2, calculated using the equation shown in figure 4.10) and m = $1.808\text{x}10^{-22}$ g, the radius of curvature of each positive Ag- ion in a gap of a magnetic circuit is then given by $r = \frac{(1.808\text{x}10^{-22}\,\text{g})(500\,\text{m/s})}{(1.6022\text{x}10^{-19}\,\text{C})(0.35\,\text{T})}$ = 1.61 mm. Similarly for a negative Ag- ion the radius of curvature is -1.61 mm.